ITTC Quality System Manual
Recommended Procedures and Guidelines

Procedure

Uncertainty Analysis for Manoeuvring Predictions based on Captive Manoeuvring Tests

7.5	Process Control
7.5-02	Testing and Extrapolation Methods
7.5-02-06	Manoeuvrability
7.5-02-06-04	Uncertainty Analysis for Manoeuvring Predictions based on Captive Manoeuvring Tests

Disclaimer

Edited	Approved
Manoeuvring Committee of the 30th ITTC	30th ITTC 2024
Date 07/2023	Date 09/2024

Table of Contents

Uncertainty Analysis for Manoeuvring Predictions based on Captive Manoeuvring Tests

1. PURPOSE OF PROCEDURE

The purpose of the procedure is to provide an example for the uncertainty analysis (UA) of a model scale towing tank planar motion mechanism (PMM) test following the ITTC Procedures 7.5-02-01-01, 'Guide to the Expression of Uncertainty in Experimental Hydrodynamics' and 7.5-02-01-06, 'Determination of type A uncertainty estimate of a mean value from a single time series measurement'.

This procedure starts with listing an extensive list of sources of uncertainties. Although exhaustive, this list is not complete and may need to be augmented based on the model basin, model set-up, and measuring equipment of every individual model test institute.

The example in Appendix A to Appendix E is based on the IIHR results of research carried out before 2008 by Yoon et al (2008). This example addresses many of the sources of the uncertainty, but not all of them. Furthermore, the worked-out example in Appendix A, only addresses the uncertainties of the measured forces and moments and does not address yet the elaboration into the uncertainty on hydrodynamic coefficients and the uncertainty of the predicted manoeuvres.

Appendix F provides an example on the uncertainty propagation from manoeuvring coefficients towards predicted manoeuvres.

Appendix G provides an elaborated example on uncertainties induced by carriage kinematics and by elaborating on the uncertainties induced by data reduction or noise.

2. SOURCES OF UNCERTAINTY

2.1 Overview

During captive manoeuvring tests, a ship model is forced by an external mechanism to undergo a prescribed trajectory in the horizontal plane. The measurement of forces acting on the model leads to the numerical value of a number of characteristic coefficients occurring in the mathematical manoeuvring model, which can be used for predicting various aspects of manoeuvring behaviour, including standard manoeuvres such as turning circle tests and zigzag tests.

The accuracy of test results is influenced by imperfections of the experimental technique.

This relates to anything which is measured, including positions, velocities and accelerations (translations and rotations) and obviously the forces and moments. The sources of uncertainties are grouped in different origins: uncertainties in the planar motion mechanism; the set-up in the basin.

2.2 Inaccuracy of ship model characteristics

The influence of some factors (e.g. uncertainties on main dimensions, offsets, loading condition) on the accuracy of test results is hard to estimate, while variations of other parameters (e.g. mass, moments of inertia) have a rather straightforward effect on the forces acting on the model:

- length;
- the individual masses;
- the placement of the individual masses (because this determines the position of the centre of gravity and the radii of inertia);
- the draft mark as drawn on the model;
- loading of the model to the draft mark;
- rudder and propeller manufacturing accuracy;
- model alignment;
- rudder alignment;
- rudder angle setting;
- propeller rate setting for the tests;
- propeller rate measurement;
- water density (as a function of water temperature).

2.3 Planar Motion Mechanism geometry discrepancies

The geometry of the planar motion mechanism and, therefore, the trajectory of the ship model may be influenced by elastic deformation, backlash and mechanical imperfections, causing geometrical uncertainties which may affect model kinematics and dynamics.

A detailed analysis highly depends on the type and concept of the mechanism. Following factors may be of importance in the case of a PMM system with three degrees of freedom:

- deviations of the main carriage with respect to the tank:
  - horizontal deviations of the main carriage's guiding rail;
  - backlash between guiding rail and horizontal guiding wheels;
  - accuracy of the guiding wheels (radius, eccentricity, backlash);
  - vertical deviations of both rails;
  - accuracy of the main carriage's wheels (radius, eccentricity, backlash);
- deviations of the lateral carriage with respect to the main carriage:
  - alignment of guiding for lateral carriage;
  - the guiding for lateral carriage with respect to main carriage should be perpendicular;
  - backlash of guiding for lateral carriage;
- deviations of the rotation table with respect to the lateral carriage:
  - alignment of rotation axis;
  - verticality of guiding for yaw table;
  - backlash;
- deviations of the model connection system with respect to the rotation table;
- inaccuracies of the connection of the ship model to the mechanism.

With respect to the latter, a distinction should be made between connection inaccuracies according to either the free or the forced motion modes. Captive model tests executed for investigation of manoeuvring of surface ships require forced surge, sway and yaw motions, while the model is usually free to heave and pitch. Roll motions may be free or forced.

Some uncertainties are caused by imperfections of the connection system:

- geometry imperfections and backlash may cause position uncertainties in all motion modes;
- mechanical friction between moving parts may result into position uncertainties in the free motion modes;
- inaccurate mounting may induce position uncertainties in all forced motions modes;

but even a perfectly functioning connection may induce position uncertainties in the forced modes due to motions in the free modes. Due to the concept of some connection systems, pitch and heave indeed induce a small surge component.

2.4 Planar Motion Mechanism control and setting uncertainties

The kinematics of the driving mechanism and, therefore, of the model are determined by a number of directly controllable parameters s_i which are either kept constant or controlled according to a time function during a test run. Setting and control uncertainties on these parameters indirectly influence the forces acting on the model. An analysis of this influence strongly depends on the concept of the mechanism and the type of test, and needs further investigation. Divergences between prescribed and actual trajectories can also be caused by inaccuracy of the measurement of position or speed of the (sub-)mechanisms, affecting the control system's feedback signal. Possible causes are:

- temperature influence;
- slip (of encoder wheel), backlash;
- uncertainties/deformation in transmission to encoder;
- resolution of encoder.

Special attention should be paid to possible limitations of the mechanism concept, which may not allow the execution of some from theoretical point of view desirable trajectories. For example, small amplitude PMM systems based on the combined action of two horizontal oscillators may not be able to perform a pure harmonic yaw motion. In other cases, limitations of the control system yield deviations from the theoretically desired trajectory: this is for instance the case if a PMM system is mounted on a towing carriage which is not equipped with a variable speed control, as this leads to fluctuations of the ship's forward speed component during a harmonic yaw test. Principally, such discrepancies are predictable and can be accounted for during analysis. The uncertainty in the PMM amplitude(s) (position or velocity) can be estimated from the standard deviation of the dataset to a Fourier fit through the data set.

Appendix G shows an elaborated example on the propagation of PMM uncertainties.

2.5 Uncertainties on ship control equipment parameters

During a test run, a number of control equipment parameters (propeller rpm, rudder angle, ...) are controlled; setting or control uncertainties have a direct influence on the forces acting on the model.

2.6 Measurement accuracy

The quality of force measurements may be affected by non-linearity, hysteresis, sensitivity, accuracy of calibration, ... Uncertainties on position and speed measurements not only affect the mechanism's control loop (see above), but also the interpretation of the measured forces.

2.7 Undesired facility related hydrodynamic effects

A ship model's dynamics and, therefore, test results may be affected by several influences caused by the limitations of the experimental facility, so that tests are not performed in unrestricted still water. Some examples:

- Residual motion of the water in the tank may affect the model's dynamics if the waiting time between two runs is too short.
- Unsteady phenomena occurring during transition between acceleration and steady phases or if harmonical techniques are applied may also affect the model's dynamics.
- Tank width and also length limitations induce undesired additional forces.
- In shallow water tests, bottom profile variations affect the model's dynamics.

The influence of these effects on the accuracy of test results generally increases with decreasing water depth. Although complete prevention is principally impossible, the effects can be reduced by an adequate selection of test and analysis parameters.

2.8 Data acquisition

Deformation of the measured signals may be induced by signal processing techniques, due to characteristics of e.g. filters, AD-conversion (resolution, time step).

2.8.1 AD-conversion

The conversion from an analogue signal to a digital signal is governed by a resolution or least significant bit (LSB), which is given by (with range typically the measured voltage):

$$LSB = \frac{Range}{2^{bit}} \quad (1)$$

For instance, the measurement range could be 20 Volt. As the quantization is now mostly 16 bits or more, the AD-conversion only induces a negligible uncertainty. Care should be taken for converters which have a quantization below 16 bits.

The LSB uncertainty is mostly expressed as $\pm 0.5 LSB$.

2.8.2 Time step

The time step has to be sufficiently small (or the sampling rate should be sufficiently large) to capture all manoeuvring effects. In practice sampling rates between 10 Hz and 1000 Hz have been reported with 50 Hz and 100 Hz as most frequently used values. The sampling rate has to be at least twice the filter rate.

2.8.3 Analogue filters

An analogue filter is used to smooth a measured signal. There are a few reasons to do this:

- To have a better graphical representation of the signal, but at the same time this does not always improve the accuracy of the measurement (see 2.9.1);
- To remove high frequency noise (so-called blue noise, to be investigated in the frequency domain), which may deteriorate the signal to noise ratio of the low frequency manoeuvring components due to the “aliasing” effects;
- To condense oversampled signals, for instance when applying a 1 kHz sampling rate.

Analogue low pass filters (or online filters) should be applied to smoothen the measured signal when unwanted harmful noise exists. Although care is needed when applying this technique:

- The transfer function characteristics have to be known. In particular, the cut off frequency and the transition band are of importance, see Figure 1.
- Care should be taken that the governing manoeuvring (or PMM) frequency is on the low pass side of the transition band (no filtering of relevant frequency range).
- The filter is never perfectly real time and a time delay is therefore introduced.
- Even in the passing band, signal variations may occur due to gain differences which depend on the filter design, see Figure 1.
- Additional noise can be induced by the filter.
- Actual noise can be hidden by the filter and should be accounted for during the uncertainty propagation (see 2.9).

For these reasons, applying a software filter (or offline filter) in post processing should be considered.

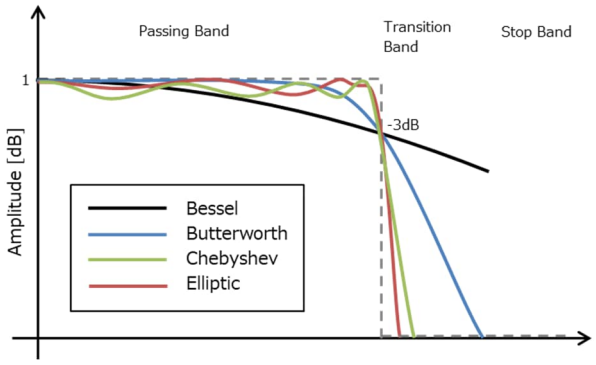

Figure 1. Amplitude response of an ideal filter and actual filters

2.9 Post-model test numerical analysis

2.9.1 Uncertainty propagation due to noise

After the execution of the model tests, the time traces are processed to obtain the average of signals or the *in- and out of phase* of signals. In most cases, this means that the noise traces are removed; however, these also contribute to the uncertainty of the signal. For instance, 7.5-02-01-06, 'Determination of type A uncertainty estimate of a mean value from a single time series measurement' gives the uncertainty of the mean of a noisy signal.

As indicated by Delefortrie and Kishimoto (2019), when performing PMM tests, this uncertainty is propagated towards the higher order harmonics of a Fourier analysis applied on the test results. The method they propose is to multiply the type A uncertainty for the mean (or the 0^{th} harmonic) as described in procedure 7.5-02-01-06 by $\sqrt{2}$ to obtain the uncertainty of all higher order harmonics (or the *in phase* and *out of phase amplitudes*).

Procedure 7.5-02-01-06 can only be applied to a stationary noise signal. If this is not the case, more advanced techniques, such as Monte Carlo simulations, are needed to investigate the uncertainty propagation of the noise into the Fourier components. Alternatively, Delefortrie and Kishimoto (2019) presented the hypothesis of an equivalent Gaussian white noise distribution which has the same area as the real spectral noise distribution. This method seems to slightly overpredict the obtained uncertainty.

If the measurement has been subjected to an analogue filtering process, as described in 2.8.3, the above-described method will underestimate the actual noise uncertainty (which does not disappear with the filtering). Therefore, it is advisable to multiply the uncertainty by the filter cut-off ratio. For example, if the signal is originally measured at 10 Hz and a 1 Hz LP filter is applied, the cut-off ratio is $10 \div 1$ and the noise uncertainty of the filtered signal should be multiplied by 10.

2.9.2 Hydrodynamic derivatives

The hydrodynamic effect of the manoeuvring is determined by subtracting the inertial and centrifugal components from the time traces. In particular, the uncertainties in the correction for the force and moment for the rotational velocity will need to be addressed.

The accuracy of calculated average values and harmonics appears to depend on the test parameters, e.g. integration length, test frequency and number of cycles.

2.9.3 Data fitting uncertainty

Fitting the results of all tests will also result in an uncertainty, which is called a data-fitting uncertainty. This depends on the selected math-

ematical model used for the simulations. An example of the effect of the data-fitting uncertainty is given in Appendix F.

3. UNCERTAINTY OF THE PREDICTIONS

The total uncertainty of the manoeuvring predictions based on the measured forces and moments during captive model tests, is the result of a set of Monte Carlo simulations.

- In a first step the uncertainty of forces and moments for drift angles, rate of turn, rudder angles, and combinations of these settings must be derived. This part is elaborated in the example described in Appendix A. Possible uncertainties induced by data acquisition and post numerical treatment need to be addressed as well.

For the determination of the total uncertainty of the manoeuvring predictions from a mathematical model a sensitivity analysis is then recommended. A sensitivity analysis is used to determine the influence and also the importance of the predicted hydrodynamic coefficient on manoeuvring performance. This should be done through analysis of simulations performed with systematic variations of each term.

The sensitivity of the ship's response *can* be identified by variation of the hydrodynamic coefficients by means of a set of Monte Carlo simulations. These variations should be conducted in the boundaries of the *(determined standard deviations of the measurements/)* derived uncertainties in section 2.

Based on the uncertainty of every measured force and moment, using the Monte Carlo approach, multiple fits can be made. Every fit is a unique combination of hydrodynamic coefficients corresponding to a selected mathematical model (See Figure 2). An example is elaborated by Woodward (2013).

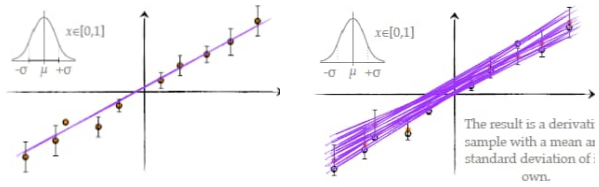

Figure 2 Monte Carlo approach of multiple fits in the boundaries of standard deviation. (Woodward, 2013)

The Monte Carlo approach of the multiple fits should be controlled by the Probability Distribution Function (PDF), see Figure 3, i.e. larger deviations of the means must be less probable.

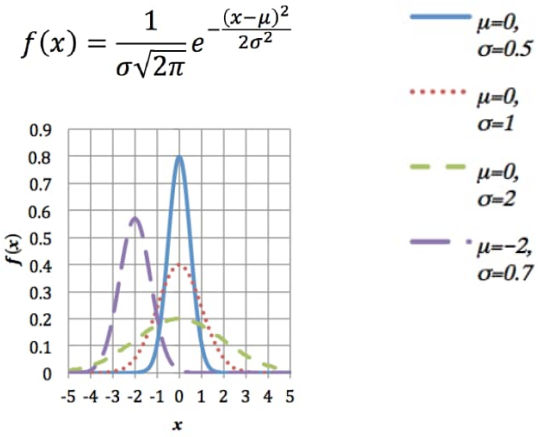

Figure 3 Definition of the PDF for various mean and standard deviations (Woodward, 2013)

On the basis of the multiple fits, simulations of standard manoeuvres (i.e. turning circle, zigzag manoeuvre) for each of these multiple fits should be carried out. Analysis of the time traces allow key parameters to be obtained, such as tactical diameters (from turning circle tests) or overshoot angles (from zigzag tests). This will hence result in a distribution of tactical diameters and overshoot angles. The analysis of the PDF of the key parameters will determine the uncertainty of these key parameters (i.e. tactical

diameters and overshoot angles) depending of the uncertainty of the hydrodynamic coefficients (See Figure 4).

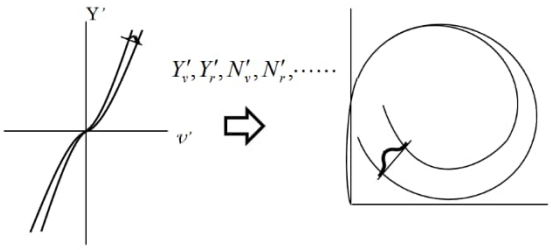

Figure 4 PDF in the measured forces results in a PDF in the key parameters of manoeuvres

Generally, the sensitivity of simulated manoeuvres to each mathematical parameter will depend on the following items (ITTC MC, 1999):

- the mathematical model itself.
- the hydrodynamics of the ship.
- the manoeuvre that is investigated, i.e. turning circle, zigzag or other manoeuvres.

An elaborated example of this is provided in Appendix F.

4. REFERENCES

Benedetti, L., Bouscasse, B., Broglia, R., Fabbri, L., La Gala, F., and Lugni, C., 2006, "PMM Model Test with DDG51 Including Uncertainty Assessment," INSEAN Report No. 14, 174 pp.

Delefortrie, G. and Kishimoto, T., 2019, "The uncertainty induced by noise and filtering on the results of captive PMM tests", AMT 2019, Rome, Italy.

ITTC, The Manoeuvring Committee, 1999, "Final Report and Recommendations to the 22nd ITTC", 51pp.

Simonsen, C., 2004, "PMM Model Test with DDG51 Including Uncertainty Assessment," FORCE Technology Report No. ONRII187 01, 145 pp.

Woodward, M. D., 2013, "Propagation of Experimental Uncertainty from Force Measurements into Manoeuvring Derivatives," AMT Conference, Poland.

Woodward, M. D., 2014, "Evaluation of Interfacility Uncertainty for Ship Manoeuvring Performance Prediction," Ocean Engineering, Vol. 88, pp. 598-606.

Yoon, H.-S., Longo, J., Toda, Y., and Stern, F., 2008, "PMM Tests and Uncertainty Assessment for Surface Combatant Including Comparisons Between Facilities," IIHR – Hydroscience & Engineering Report

Appendix A.
EXAMPLE OF UNCERTAINTY OF MEASURED FORCE DURING PMM CAPTIVE DRIFT TEST AND OSCILLATION TEST

The present example is developed in collaboration between IIHR-Hydroscience & Engineering (IIHR), FORCE Technology, Instituto Nazionale per Studi ed Esperienze di Architettura Navale (INSEAN), and the 24th – 25th ITTC Manoeuvring Committee, including overlapping tests using the same model geometry for comparison of results and identification of facility biases and scale effects. Details of the UA procedures are provided by Simonsen (2004), Benedetti et al. (2006), and Yoon et al. (2007), including in the latter case comparisons between facilities and analysis of facility biases, scale effects, and parameter trends. Since at the time of writing this example, the state-of-the-art was not ISO GUM, many of the wordings in the example are related to bias and precision limits, instead of the later preferred type A and type B uncertainties.

This example provides an uncertainty assessment for a model scale towing tank PMM test for an un-appended model ship except bilge keels (i.e. without shafts, struts, propellers, and rudders) which is mounted free to heave and pitch but fixed in roll. The PMM test conforms to the ITTC Procedures 7.5-02-06-02, 'Captive Model Test Procedure.' Uncertainties for multiple runs are estimated for the non-dimensional forces and moment in model scale for four types of PMM tests (static drift, pure yaw, pure sway, and yaw and drift) at one Froude number (Fr = 0.280). Other PMM tests, such as static rudder, static drift and rudder, static drift and heel, dynamic yaw and rudder, dynamic yaw and drift and rudder, are not considered. This example does not provide UA for hydrodynamic derivatives derived from the forces and moment data or their effect on the full-scale manoeuvring simulations. The latter is performed in Appendix F, based on a different data set. Additionally, UA estimates for heave and pitch are not provided.

The effect of data conditioning such as filtering or fairing, for example, Fourier series reconstructions for the measured forces /moment and motions is not counted in this UA procedure. This procedure assumes that the measured forces/moment is the sum of those from all forces/moment gauges used for the case of multiple gauge system, and that the inertia forces/moment from parts for model installation are subtracted from the total measured forces and moments if the parts are suspended from the load cells. This procedure also assumes that the model ship is free to heave and pitch and fixed in roll. The effect of deviations from the upright position such as roll or heel angle is not considered in this procedure. Finally, carriage speed is assumed to be constant, so the effect of acceleration caused by fluctuating carriage speed during runs is not considered. However, bear in mind that a fluctuating carriage speed can have a significant effect on the results, especially if the fluctuation is equal to the test frequency during harmonic tests, as is shown in Appendix G.

A.1. Test Design

The tests are conducted in the IIHR towing tank, which is 100m long, 3.048m wide and 3.048m deep, and equipped with a drive carriage, PMM carriage, automated wave dampener system, and wave-dampening beach. A right-handed Cartesian coordinate system is fixed to the model. The origin is at the intersection of the midship plane, centre plane, and water plane. The x, y, z axes are directed upstream, transversely to starboard, and downward, respectively (See Figure A1).

The model geometry is DTMB model 5512, a 1:46.6 scale, L_{PP} = 3.048 m. The model is un-

appended except for port and starboard bilge keels, i.e., not equipped with shafts, struts, propulsors, or rudders.

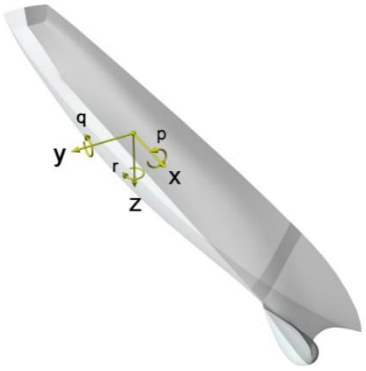

Figure A1 Coordinate system.

To initiate transition to turbulent flow, a row of cylindrical studs of 1.6 mm height and 3.2 mm diameter are fixed with 9.5 mm spacing at x/L_{PP} = 0.45. The stud dimensions and placement on the model are in accordance with the recommended procedure 7.5-01-01-01. Model- and full-scale geometric parameters for 5512 are summarized in Table A1.

Table A1 Full and model scale particulars.

		Ship	Model
λ	-	1 : 1	1 : 46.588
L_{PP}	m	142.00	3.048
L_{WL}	m	142.18	3.052
B_{WL}	m	19.10	0.410
T_m	m	6.16	0.136
∇	m^3	8472	0.084
Δ	Ton	8684	0.086
C_B	-	0.506	0.506
A_{WP}	m^2		0.979
m	kg		82.55
x_G	m		-0.0157
y_G	m		0.0000
I_z	$kg{\cdot}m^2$		49.99

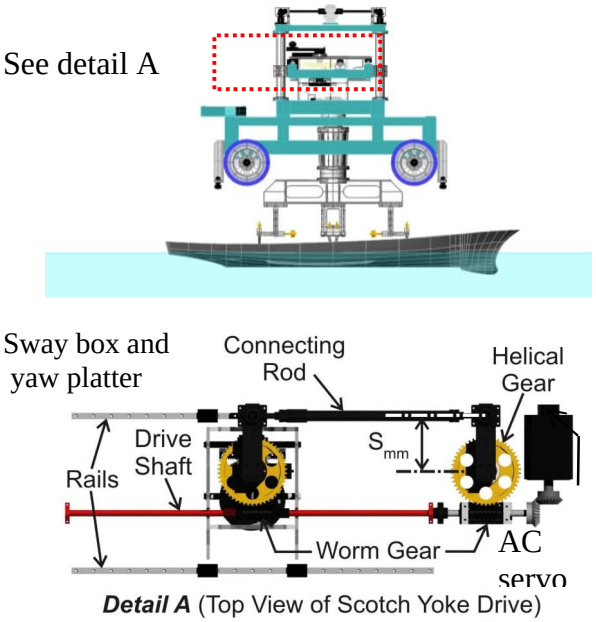

Figure A2 Side view of the PMM carriage and model ship mount (top), and close up of the scotch yoke drive (bottom).

The model is ballasted with respect to port and starboard draft markers, and then connected to a mount with three ball-bearing type contacts which allows the model to move freely in pitch and heave, but constrains roll motion (See Figure A2). The mount is suspended from the load cell which is fixed at the PMM carriage. The mass and yaw moment of inertia of the mount are measured to correct their effects on the measured forces and moment at the date reductions phase of the test.

Table A2 Test conditions for static drift test.

Fr [-]	U_C [m/s]	β [deg.]	v' [-]
0.280	1.531	-10	-0.174

$$v' = \frac{v}{U_C}$$

Table A3 Test conditions for pure sway test.

Fr [-]	U_C [m/s]	β_{corr} [deg]	N [rpm]	S_{mm} [m]	v'_{max} [-]	$\dot{v}'_{max}$ [-]
0.280	1.531	10	8.0210	0.1584	0.174	0.291

$$\beta_{corr} = \frac{v_{max}}{U}, v'_{max} = \frac{v_{max}}{U}, \dot{v}'_{max} = \frac{\dot{v}_{max} L_{PP}}{U}$$

Table A4 Test conditions for pure yaw test.

Fr [-]	U_C [m/s]	N [rpm]	S_{mm} [m]	ψ_0 [deg.]	r'_{max} † [--]	$\dot{r}'_{max}$ [--]
0.280	1.531	8.0210	0.1636	10.2	0.30	0.50

$$r'_{max} = \frac{r_{max} L_{PP}}{U} \; \dot{r}'_{max} = \frac{\dot{r}_{max} L_{PP}^2}{U^2}$$

Table A5 Test conditions for yaw and drift test.

Fr [-]	U_C [m/s]	β [deg]	N [rpm]	S_{mm} [m]	ψ_0 [deg]	r'_{max} [--]	$\dot{r}'_{max}$ [--]
0.280	1.531	10	8.0210	0.1636	10.2	0.30	0.50

Static drift test is conducted at the drift angle $\beta = -10°$; pure sway test at the corresponding drift angle $\beta_{corr} = 10°$; pure yaw test at $r'_{max} = 0.3$; and yaw and drift test at the same yaw rate of the pure yaw test with a drift angle $\beta = 10°$. The details of each test condition are presented in Tables A2-A5. Test conditions in the present procedure are a part of the full test matrix in Yoon et al. (2007).

A.2. Data Acquisition and Reduction

The present interest is in data acquisition of carriage speed U_C, ship model motions (y, ψ), and forces and moments (F_x, F_y, M_z) for static and dynamic PMM tests. All variables are acquired as time histories through each carriage run. Static test variables (F_x, F_y, M_z) are time-averaged whereas dynamic test variables (y, ψ, F_x, F_y, M_z) are treated with harmonic analysis in the data reduction phases of the study. The measurement details for U_C are presented in Longo and Stern, (2005).

If it is assumed that the vessel moves in the horizontal plane only (surge, sway, and yaw), the motion equations are reduced to the following equations:

$$\begin{aligned} -F_x + X &= m(\dot{u} - vr - x_G r^2 - y_G \dot{r}) \\ -F_y + Y &= m(\dot{v} + ur - y_G r^2 + x_G \dot{r}) \\ -M_z + N &= I_z \dot{r} + m\big(x_G(\dot{v} + ur) - y_G(\dot{u} - rv)\big) \end{aligned} \quad \text{(A1)}$$

where, X, Y, N are the hydrodynamic forces and moment, m is the mass of the model ship, I_z is the yaw moment of inertia of the model ship, x_G is the longitudinal distance from midship to model ship centre of gravity (COG), y_G is the transverse distance from centerplane to model ship COG, u, v, r are surge, sway, yaw velocities, respectively, $\dot{u}$, $\dot{v}$, $\dot{r}$ are surge, sway, yaw accelerations, respectively. In general $y_G = 0$ for conventional marine vessels, but it is assumed to be non-zero for the purpose of uncertainty assessment. Equations (A1) can be made non-dimensional using water density ρ, advance speed $U = \sqrt{u^2 + v^2}$, mean draft T_m, and ship model length L_{PP}. The non-dimensional variables are denoted with a prime symbol and represent the data reduction equations (DRE's) for the measurements herein.

$$X' = \frac{F_x + m(\dot{u} - vr - x_G r^2 - y_G \dot{r})}{(1/2)\rho U^2 T_m L_{PP}} \quad \text{(A2)}$$

$$Y' = \frac{F_y + m(\dot{v} + ur - y_G r^2 + x_G \dot{r})}{(1/2)\rho U^2 T_m L_{PP}} \quad \text{(A3)}$$

$$N' = \frac{M_z + I_z \dot{r} + m\big(x_G(\dot{v} + ur) - y_G(\dot{u} - rv)\big)}{(1/2)\rho U^2 T_m L_{PP}^2} \quad \text{(A4)}$$

Although equations (A2-A4) are technically applicable DRE's for all tests herein, they can be simplified considerably by dropping the inertia terms for the case of the static drift tests which is done below in equations (A5-A7).

$$X' = \frac{F_x}{(1/2)\rho U_C^2 T_m L_{PP}} \quad \text{(A5)}$$

$$Y' = \frac{F_y}{(1/2)\rho U_C^2 T_m L_{PP}} \quad \text{(A6)}$$

$$N' = \frac{M_z}{(1/2)\rho U_C^2 T_m L_{PP}^2} \quad \text{(A7)}$$

For static tests, average values of surge and sway forces and yaw moment are computed from the time histories. For the dynamic tests, first the inertia forces and moment of the model ship and the mount are subtracted from the measured forces and moment, respectively. Then, the resultant time histories of the forces and yaw moment are reconstructed with a 6th-order Fourier series equation using the input PMM frequency as the prime frequency of the Fourier series. Uncertainties related to the averaging and Fourier series reconstruction processes as described in 2.8 - 2.9 are not considered in the present example. The choice for a 6th order Fourier series is a choice, made in this example, because a 3rd order Fourier fit is more common. The 6th order may lead to a sensitivity of the derivatives related to small changes in the forces and may be uncertain due to noise propagation. In a fully worked out uncertainty analysis, the sensitivity to the choice of the order of the Fourier series should be taken into account.

A.3. Measurement Systems and Procedures

Three forces and three moments are measured with an Izumi six-component strain-gauge type load cell, six Izumi amplifiers, 16-channel AD converter and PC. Maximum force and moment ranges are 500 N for F_x, F_y, F_z and 50 Nm, 50 Nm, 200 Nm for M_x, M_y, M_z, respectively.

Ship model motions are measured using a Krypton Electronic Engineering Rodym DMM motion tracker. The Rodym DMM is a camera-based measurement system that triangulates the position of a target in 3D space for contactless measurement and evaluation of 6DOF motions. The hardware consists of a camera module comprising three fixed CCD cameras, target with 1-256 light-emitting diodes (LED's), camera control unit, hand-held probe with six LED's, and PC. Krypton software is used for system calibration, and data acquisition and reduction.

Carriage speed is measured with an IIHR-designed and built speed circuit. The operating principle is integer pulse counting at a wheel-mounted encoder. The hardware consists of an 8000-count optical encoder, carriage wheel, sprocket pair and chain, analogue-digital (AD) converter, and PC. Linear resolution of the encoder, sprocket pair and chain, and wheel assembly is 0.15 mm/pulse. The speed circuit is periodically bench-calibrated to determine and adjust the frequency input/voltage output transfer function.

A four-wheel carriage supports the main PMM mechanical system which is towed behind the IIHR drive carriage. The mechanical system is a scotch-yoke type which converts rotational motion of an 11 kW AC servo motor to linear sway motion of a sway box and angular yaw motion of a yaw platter beneath the sway box (See Figure A2). The scotch-yoke is driven through a control rack, PC, and software up to 0.25 Hz with maximum sway and yaw amplitudes of ±500 mm and ±30°, respectively. A strongback (1.5 m) is attached to the yaw platter, which is pre-settable at a drift angle between ±30° for static drift or combined yaw and drift tests. Factory calibrated linear and rotational potentiometers are installed on the carriage to monitor and report the sway and yaw position of the sway box and yaw platter, respectively.

For static drift tests, the ship motion is defined by the towing speed U_C and the specified drift angle β relative to the towing direction. For dynamic tests, the ship motion is imposed to control velocities (surge u, sway v, yaw r), and accelerations (surge $\dot{u}$, sway $\dot{v}$, yaw $\dot{r}$) in the local ship system at any given instant (See Figure A3).

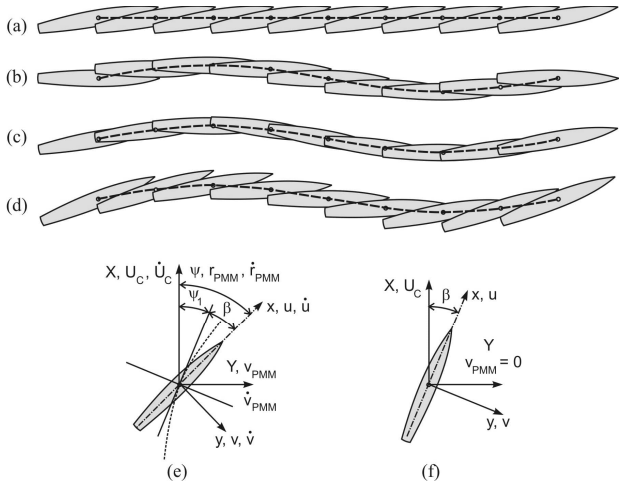

Figure A3 Definitions of PMM tests and motion parameters: (a) static drift; (b) pure sway; (c) pure yaw; (d) yaw and drift; (e) dynamic test motion parameters; (f) static test motion parameters.

Dynamic test ship motions are composed of:

1. carriage speed, U_C;
2. PMM-generated transverse oscillation of the model from side to side (perpendicular to the towing direction) defined by the velocity v_{PMM} and the acceleration $\dot{v}_{PMM}$;
3. PMM-generated horizontal rotation from side to side of the model around a vertical axis through the midship, defined by the angular velocity r_{PMM} and the angular acceleration $\dot{r}_{PMM}$ and
4. a drift angle β if the yaw and drift condition is considered (Figure A3). The time-dependent PMM motion parameters can differ from facility to facility, but those for the current example are described basically by three quantities. These include the sway crank amplitude S_{mm}, yaw motion amplitude ψ_0, and PMM frequency $\omega = 2\pi N/60$, where N is the number of PMM rotations per minute. The following relations are used to setup static and dynamic tests according to the test conditions in Tables A2-A5:

Heading:

$$\psi = \psi_0 \cos\omega t + \beta \quad \text{(A8)}$$

Yaw rate:

$$r_{PMM} = -\psi_0 \omega \sin\omega t \quad \text{(A9)}$$

Yaw acceleration:

$$\dot{r}_{PMM} = -\psi_0 \omega^2 \cos\omega t \quad \text{(A10)}$$

Transverse translation:

$$\eta_{PMM} = -2S_{mm} \sin\omega t \quad \text{(A11)}$$

Transverse velocity:

$$v_{PMM} = -2\omega S_{mm} \cos\omega t \quad \text{(A12)}$$

Transverse acceleration:

$$\dot{v}_{PMM} = 2\omega^2 S_{mm} \sin\omega t \quad \text{(A13)}$$

where, η_{PMM} in (A11) is the transverse position of the model ship in towing tank coordinates. If a different PMM motion generation mechanism is used, equations (A8-A13) should be replaced with the appropriate PMM motion equations.

The motion parameters of the model ship moving in a ship-fixed moving frame of reference can be expressed with the above PMM motion parameters. The carriage acceleration is assumed to be zero, i.e. $\dot{U}_C = 0$ in the following equations.

Sway velocity:

$$v = v_{\mathrm{PMM}}\cos\psi - U_{\mathrm{C}}\sin\psi \quad \text{(A14)}$$

Sway acceleration:

$$\dot{v} = \dot{v}_{\mathrm{PMM}}\cos\psi - r(U_{\mathrm{C}}\cos\psi + v_{\mathrm{PMM}}\sin\psi) \quad \text{(A15)}$$

Yaw rate:

$$r = r_{\mathrm{PMM}} \quad \text{(A16)}$$

Yaw acceleration:

$$\dot{r} = \dot{r}_{PMM} \quad \text{(A17)}$$

Surge velocity:

$$u = U_C\cos\psi + v_{\mathrm{PMM}}\sin\psi \quad \text{(A18)}$$

Surge acceleration:

$$\dot{u} = \dot{v}_{\mathrm{PMM}}\sin\psi + \\ +r(v_{\mathrm{PMM}}\ cos\psi - U_C\ \sin\psi) \quad \text{(A19)}$$

A.4. Uncertainty Analysis

The uncertainty analysis procedures are based on estimates of type A and type B, and their root-sum-square (RSS) combination to ascertain expanded uncertainty (U). UA is applied to data reduction equations (A2-A4) for dynamic tests and (A5-A7) for static tests, respectively, which are written in functional forms below (A20-A22) for dynamic tests and (A23-A25) for static tests, respectively.

$$X' = X'\begin{pmatrix} L_{\mathrm{PP}}, T_{\mathrm{m}}, x_{\mathrm{G}}, y_{\mathrm{G}}, m, \rho, \\ u, v, r, \dot{u}, \dot{r}, F_x \end{pmatrix} \quad \text{(A20)}$$

$$Y' = Y'\begin{pmatrix} L_{\mathrm{PP}}, T_{\mathrm{m}}, x_{\mathrm{G}}, y_{\mathrm{G}}, m, \rho, \\ u, v, r, \dot{v}, \dot{r}, F_y \end{pmatrix} \quad \text{(A21)}$$

$$N' = N'\begin{pmatrix} L_{\mathrm{PP}}, T_{\mathrm{m}}, x_{\mathrm{G}}, y_{\mathrm{G}}, m, I_Z, \rho, \\ u, v, r, \dot{u}, \dot{v}, \dot{r}, M_z \end{pmatrix} \quad \text{(A22)}$$

$$X' = X'(L_{\mathrm{PP}}, T_{\mathrm{m}}, \rho, U_{\mathrm{C}}, F_x) \quad \text{(A23)}$$

$$Y' = Y'(L_{\mathrm{PP}}, T_{\mathrm{m}}, \rho, U_{\mathrm{C}}, F_y) \quad \text{(A24)}$$

$$N' = N'(L_{\mathrm{PP}}, T_{\mathrm{m}}, \rho, U_{\mathrm{C}}, M_z) \quad \text{(A25)}$$

Type B uncertainty is estimated with consideration of elemental uncertainty sources for individual variables, whereas type A uncertainty is estimated end to end. The expanded uncertainty is achieved through careful estimation of type B uncertainties and usage of a large sample, multiple test approach for type A uncertainties. The sources of uncertainty for PMM tests are shown in Figure A4.

A.5. Standard uncertainties (U)

Fourteen standard uncertainties U_x, where $x = L_{\mathrm{PP}}, T_{\mathrm{m}}, x_{\mathrm{G}}, y_{\mathrm{G}}, m, I_Z, \rho, u, v, r, \dot{u}, \dot{v}, \dot{r}, F$ (hereafter F is either F_x, F_y, or M_z) are identified from the uncertainty propagation equations of the DRE's (A20-A22) for dynamic tests, and five standard uncertainties U_x, where $x = L_{\mathrm{PP}}$, T_{m}, ρ, U_{C}, F from (A23-A25) for static tests.

$$U_R^2 = \sum_x \theta_x^2 U_x^2 \quad \text{(A26)}$$

Sensitivity coefficients $\theta_x = \partial R/\partial x$ (hereafter R is either X', Y', or N') of individual variable results are evaluated analytically, and their definitions are summarized in Tables A12, A13, and A14 for $U_{X'}$, $U_{Y'}$, and $U_{N'}$, respectively. The individual uncertainties U_x are defined and estimated as below. Additional or details of estimation procedures for some variables are presented in Appendices B, C, D, and E.

The model length uncertainty is estimated as $U_{L_{\mathrm{PP}}}$= 0.002m, which corresponds to 0.07% of L_{PP}, by assuming the model ship fabrication uncertainty to be ±1 mm in all coordinates according to ITTC Procedure 7.5-01-01-01, 'Ship Models'.

U_{T_m} is composed of two uncorrelated uncertainties ($U_{T_\mathrm{m},1}$, $U_{T_\mathrm{m},2}$). $U_{T_\mathrm{m},1}$ is the marking accuracy of draft markers on the model ship surface, and assumed to be 0.1 mm. $U_{T_\mathrm{m},2}$ is from the model ship ballasting uncertainty with respect to the draft markers, which is estimated as 1 mm based on visual inspection. From the RSS of $U_{T_\mathrm{m},1}$ and $U_{T_\mathrm{m},2}$, U_{T_m} is estimated as 1 mm, which corresponds to 0.7% of T_m. The estimation procedure for the case of model ballasting based on displacement is given in Appendix B.

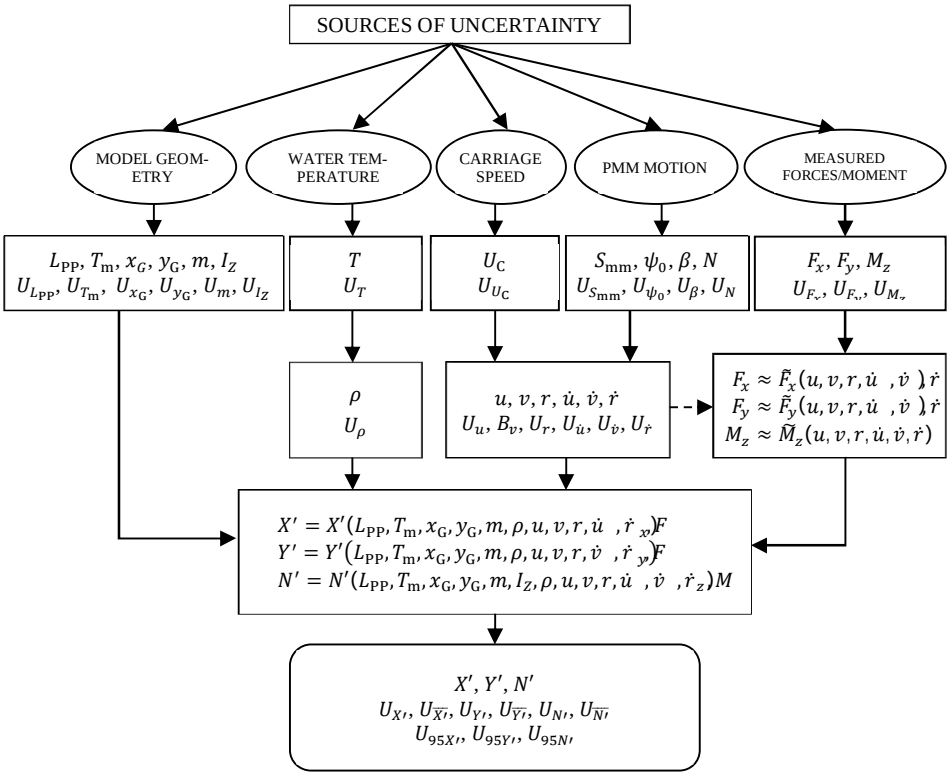

Figure A4 Sources of uncertainties in a PMM test.

The uncertainties of COG (U_{x_G}, U_{y_G}) consist of two uncorrelated uncertainties; $U_{G,1}$ and $U_{G,2}$, where the subscript G represents either x_G or y_G. $U_{G,1}$ is the model installation uncertainty and $U_{G,2}$ is the deviation of actual model COG from the designed position. Estimated U_{x_G} and U_{y_G} are summarized as follows:

Term (G)	$U_{G,1}$ [m]	$U_{G,2}$ [m]	U_G [m]
x_G	0.002	0.005	0.0054
y_G	0.001	0.002	0.0022

Total mass m of the model is calculated by summing individually measured element masses which are the bare model ship, ballast weights, and parts for model installation. Accordingly, U_m is the RSS of $U_{m,i}$'s which are the individual mass measurement uncertainties. U_m is esti-

mated as 0.11 kg (0.1% of m = 82.55 kg). Measured masses of all elements together with their uncertainties are summarized in Table A6.

Table A6 Model mass uncertainties estimation.

No. (i)	Item	m_i [kg]	$u(m_i)$ [kg]
1	Bare model ship	55.99	0.045
2	Ballast weight 1	2.27	0.023
3	Ballast weight 6	2.27	0.023
4	Ballast weight 11	2.27	0.023
5	Ballast weight 12	2.27	0.023
6	Ballast weight 13	2.27	0.023
7	Ballast weight 15	1.70	0.023
8	Ballast weight 16	1.70	0.023
9	Ballast weight 18	1.13	0.023
10	Ballast weight 19	1.09	0.023
11	Ballast weight 23	1.13	0.023
12	Ballast weight 24	0.88	0.023
13	Ballast weight A	0.20	0.023
14	Ballast weight B	0.20	0.023
15	Ballast weight C	1.36	0.023
16	Krypton target	2.47	0.023
17	Part 1	1.11	0.023
18	Part 2	1.11	0.023
19	Part 3	1.11	0.023
$m = \sum_i m_i$ = 82.55 kg			
$U_m = \sqrt{\sum_i U_{m_i}^2}$ = 0.11 kg			

From separate measurements of model ship yaw moment of inertia, U_{I_z} is estimated as 1.84 kg·m^2, which corresponds to 3.7% of the measured model yaw moment of inertia I_z = 49.79 kg·m^2. Details of I_z measurement and U_{I_z} estimation procedures are given in Appendix C.

Water density is calculated according to the ITTC procedure 7.5-02-01-03, which indicates that the water density is a function of the temperature.

Water temperature T is measured at the model mid draft with a resistive-type probe and signal conditioner. The temperature-probe accuracy is rated at U_T = ±0.2°C and $U_\rho = \sqrt{(\partial\rho/\partial T)^2 U_T^2}$ is estimated as 0.041 kg/m^3 which is 0.004% of the measured water density ρ = 998.1 kg/m^3 at 20°C.

Carriage speed uncertainty is estimated end to end by calibrating the carriage speed with respect to reference speeds. Reference speeds are obtained by measuring travel time Δt for a known distance ΔL. From the calibration U_{U_C} is estimated as 0.010m/s, which corresponds to 0.7% of carriage speed 1.531 m/s (F_r = 0.280). Details of U_C calibration and U_{U_C} estimation procedures are summarized in Appendix D.

Uncertainties of motion parameters U_v, $U_{\dot{v}}$, U_r, $U_{\dot{r}}$, U_u, $U_{\dot{u}}$ are estimated from combined uncertainty, using equations (A27-A32) through their own DRE's (A14-A19), respectively.

$$U_v^2 = \theta_{U_C}^2 U_{U_C}^2 + \theta_\psi^2 U_\psi^2 + \theta_{v_{\mathrm{PMM}}}^2 U_{v_{\mathrm{PMM}}}^2 \quad \text{(A27)}$$

$$U_{\dot{v}}^2 = \theta_{U_C}^2 U_{U_C}^2 + \theta_\psi^2 U_\psi^2 + \theta_r^2 U_r^2 + + \theta_{v_{\mathrm{PMM}}}^2 U_{v_{\mathrm{PMM}}}^2 + \theta_{\dot{v}_{\mathrm{PMM}}}^2 U_{\dot{v}_{\mathrm{PMM}}}^2 \quad \text{(A28)}$$

$$U_r^2 = \theta_{\psi_0}^2 U_{\psi_0}^2 + \theta_N^2 U_N^2 + \theta_t^2 U_t^2 \quad \text{(A29)}$$

$$U_{\dot{r}}^2 = \theta_{\psi_0}^2 U_{\psi_0}^2 + \theta_N^2 U_N^2 + \theta_t^2 U_t^2 \quad \text{(A30)}$$

$$U_u^2 = \theta_{U_C}^2 U_{U_C}^2 + \theta_\psi^2 U_\psi^2 + \theta_{v_{\mathrm{PMM}}}^2 U_{v_{\mathrm{PMM}}}^2 \quad \text{(A31)}$$

$$U_{\dot{u}}^2 = \theta_{U_C}^2 U_{U_C}^2 + \theta_\psi^2 U_\psi^2 + \theta_r^2 U_r^2 + + \theta_{v_{\mathrm{PMM}}}^2 U_{v_{\mathrm{PMM}}}^2 + \theta_{\dot{v}_{\mathrm{PMM}}}^2 U_{\dot{v}_{\mathrm{PMM}}}^2 \quad \text{(A32)}$$

where the uncertainties, U_ψ, $U_{v_{\mathrm{PMM}}}$, $U_{\dot{v}_{\mathrm{PMM}}}$ are estimated from their data reduction equations (A8), (A12), (A13), respectively.

$$U_\psi^2 = \theta_{\psi_0}^2 U_{\psi_0}^2 + \theta_N^2 U_N^2 + \theta_t^2 U_t^2 + \theta_\beta^2 U_\beta^2 \quad \text{(A33)}$$

$$U^2_{v_{\mathrm{PMM}}} = \theta^2_N U^2_N + \theta^2_{S_{\mathrm{mm}}} U^2_{S_{\mathrm{mm}}} + \theta^2_t U^2_t \quad \text{(A34)}$$

$$U^2_{\dot{v}_{\mathrm{PMM}}} = \theta^2_N U^2_N + \theta^2_{S_{\mathrm{mm}}} U^2_{S_{\mathrm{mm}}} + \theta^2_t U^2_t \quad \text{(A35)}$$

The sensitivity coefficients in (A27-A35) are evaluated analytically.

Of the five elemental uncertainties associated with motion parameters U_x, where $x = S_{\mathrm{mm}}, \beta, \psi_0$ is from the test setup and U_N, U_t are from empirical estimation, which are presented in Table A7.

Table A7 Elemental uncertainties related to the PMM motion generation.

Uncertainty	Magnitude
$U_{S_{\mathrm{mm}}}$	0.0005 m
$U_\beta = U_{\psi_0}$	0.22 deg
U_N	0.0006 rpm
U_t	0.001 sec

Drift angle uncertainty U_β is assumed to be composed of two uncorrelated elemental uncertainties $U_{\beta,\mathrm{align}}$ and $U_{\beta,\mathrm{drift}}$. $U_{\beta,\mathrm{align}}$ is the model ship installation uncertainty with respect to straight towing direction and assumed to be 0.03°. $U_{\beta,\mathrm{drift}}$ is the deviation from designated drift angle setting and estimated end to end by calibrating the drift angle with respect to reference angles, and estimated as 0.22°. Details of drift angle calibration and U_β estimation procedures are presented in the Appendix E. The uncertainty of the maximum heading angle of yaw motion U_{ψ_0} is assumed to be same as U_β.

Uncertainties of measured forces/moment U_F, where F is either F_x, F_y, or M_z, is composed of 9 uncorrelated elemental uncertainties for dynamic tests

$$U^2_F = U^2_{F,\mathrm{calib}} + U^2_{F,\mathrm{acquis}} + U^2_{F,u} + U^2_{F,\dot{u}} + \\ + U^2_{F,v} + U^2_{F,\dot{v}} + U^2_{F,r} + U^2_{F,\dot{r}} + U^2_{F,t} \quad \text{(A36)}$$

and 4 uncorrelated elemental uncertainties for static tests.

$$U^2_F = U^2_{F,\beta} + U^2_{F,\mathrm{align}} + U^2_{F,\mathrm{calib}} + U^2_{F,\mathrm{acquis}} \quad \text{(A37)}$$

$U_{F,\beta}$ and $U_{F,\mathrm{align}}$ are from drift angle setting uncertainty and uncertainty of alignment of ship model with respect to straight towing direction, respectively. Estimation procedures and results of $U_{F,\beta}$ and $U_{F,\mathrm{align}}$ are summarized in Table A8.

Table A8 $U_{F,\beta}$ and $U_{F,\mathrm{align}}$ estimations.

ε_β [rad]	$\varepsilon_{\mathrm{align}}$ [rad]	β = -10°		
3.84× 10^{-3}	5.24× 10^{-4}	$\frac{dF_x}{d\beta}$	$U_{F_x,\beta}$	$U_{F_x,\mathrm{align}}$
		[N/rad]	[N]	[N]
		30.2	0.1161	0.0158
		$\frac{dF_y}{d\beta}$	$U_{F_y,\beta}$	$U_{F_y,\mathrm{align}}$
		[N/rad]	[N]	[N]
		209.9	0.8061	0.1100
		$\frac{dM_z}{d\beta}$	$U_{M_z,\beta}$	$U_{M_z,\mathrm{align}}$
		[Nm/rad]	[Nm]	[Nm]
		283.9	1.0903	0.1488
$U^2_{F,\beta} = \left(\frac{dF}{d\beta}\right)^2 \varepsilon^2_\beta$, $U^2_{F,\mathrm{align}} = \left(\frac{dF}{d\beta}\right)^2 \varepsilon^2_{F,\mathrm{align}}$; $F = F_x, F_y$, or M_z				

Sensitivity coefficients $\partial F/\partial\beta$'s are obtained from static drift test results. $U_{F,\mathrm{calib}}$ is the RSS of the uncertainties of individual weights used for forces/moment gauge calibration.

Estimation procedures and measurement results of $U_{F,\text{calib}}$ are summarized in Table A9.

Table A9a $U_{F_x,\text{calib}}$ and $U_{F_y,\text{calib}}$ estimation.

F_x weight, w_i [N]	$\varepsilon_{w,i}$ [N]	F_y weight, w_i [N]	$\varepsilon_{w,i}$ [N]
9.81	0.00020	4.90	0.00010
14.71	0.00029	9.81	0.00020
19.61	0.00039	14.71	0.00029
49.03	0.00098	19.61	0.00039
-	-	49.03	0.00098

$U_{F,\text{calib}} = \sqrt{\sum_i \varepsilon_{w,i}^2}$

$U_{F_x,\text{calib}} = U_{F_y,\text{calib}} = 0.001\text{N}$

Table A9b $U_{M_z,\text{calib}}$ estimation.

weight, w_i [N]	$M_{z,\text{calib},i}$ [Nm]	ε_{w_i} [N]	$U_{M_z,\text{calib},i}$ [Nm]
4.90	2.24	0.00010	0.00245
9.81	4.48	0.00020	0.00490
14.71	6.73	0.00029	0.00736
19.61	8.97	0.00039	0.00981
49.03	22.42	0.00098	0.02452

$L_{\text{calib}} = 0.4572\text{m}$, $\varepsilon_{L_{\text{calib}}} = 0.0005\text{m}$

$M_{z,\text{calib},i} = w_i \times L_{\text{calib}}$

$$U_{M_z,\text{calib},i}^2 = \left(\frac{\partial M_{z,\text{calib},i}}{\partial w_i}\right)^2 \varepsilon_{w_i}^2 + \left(\frac{\partial M_{z,\text{calib},i}}{\partial L_{\text{calib}}}\right)^2 \varepsilon_{L_{\text{calib}}}^2 = L_{\text{calib}}^2 \varepsilon_{w_i}^2 + \varepsilon_{w_i}^2 \varepsilon_{L_{\text{calib}}}^2$$

$U_{M_z,\text{calib}} = \sqrt{\sum_i U_{M_z,\text{calib},i}^2} = 0.028\text{Nm}$

Table A10 $U_{F,\text{acquis}}$ estimation.

F_x		F_y		M_z	
$\lvert F_x \rvert$ [N]	$\lvert\overline{\Delta F_x}\rvert_{\max}$ [N]	$\lvert F_y \rvert$ [N]	$\lvert\overline{\Delta F_y}\rvert_{\max}$ [N]	$\lvert M_z \rvert$ [Nm]	$\lvert\overline{\Delta M_z}\rvert_{\max}$ [Nm]
9.81	0.0282	9.81	0.0262	8.97	0.0352
14.71	0.0407	19.61	0.0558	14.93	0.0494
19.61	0.0571	39.23	0.1334	26.90	0.0782
29.42	0.0769	58.84	0.2009	35.87	0.1045
49.03	0.1326	78.45	0.2767	44.84	0.1389

$\lvert\overline{\Delta F}\rvert_{\max} = \lvert\overline{\Delta F}\rvert + U_{\lvert\overline{\Delta F}\rvert}$

$U_{\lvert\overline{\Delta F}\rvert} = \frac{2S_{\lvert\overline{\Delta F}\rvert}}{\sqrt{M}}$, $S_{\lvert\overline{\Delta F}\rvert} = \left[\sum_{i=1}^{M} \frac{(\lvert\Delta F_i\rvert - \lvert\overline{\Delta F}\rvert)^2}{M-1}\right]^{\frac{1}{2}}$

$\overline{\Delta F} = \frac{1}{M}\sum_{i=1}^{M}\lvert\Delta F_i\rvert$, $\Delta F_i = F_{\text{measured},i} - F_{\text{applied},i}$

M : number of repeats = 12

$U_{F_x,\text{acquis}} = 0.002634\lvert F_x\rvert + 0.002534$

$U_{F_y,\text{acquis}} = 0.003668\lvert F_y\rvert + 0.001245$

$U_{M_z,\text{acquis}} = 0.002927\lvert M_z\rvert + 0.002505$

$U_{F,\text{acquis}}$ is from the volt-to-force conversion uncertainty of the forces/moment measurement gauges. Estimation procedures and measurement results of $U_{F,\text{acquis}}$ are summarized in Table A10. These are based on repeat tests.

Other standard uncertainties $U_{F,u}$, $U_{F,\dot{u}}$, $U_{F,v}$, $U_{F,\dot{v}}$, $U_{F,r}$, $U_{F,\dot{r}}$, $U_{F,t}$ are calculated by applying the uncertainty propagation equation to measured forces and moment F by assuming F is a function of motion parameters (u, v, r, $\dot{u}$, $\dot{v}$, $\dot{r}$) and time (t),

$$U_{F,x} = \frac{\partial F}{\partial x} U_x \qquad \text{(A38)}$$

where $x = u, v, r, \dot{u}, \dot{v}, \dot{r}, t$.

Table A11 Definitions of polynomial models.

Pure yaw	$\tilde{F}_x = X_0 + X_u u + X_r r + X_{rr} r^2 + X_{\dot{u}} \dot{u} + X_{\dot{r}} \dot{r} + X_v v + X_{\dot{v}} \dot{v}$ $\tilde{F}_y = Y_0 + Y_u u + Y_r r + Y_{rrr} r^3 + Y_{\dot{u}} \dot{u} + Y_{\dot{r}} \dot{r} + Y_v v + Y_{\dot{v}} \dot{v}$ $\tilde{M}_z = M_0 + M_u u + M_r r + M_{rrr} r^3 + M_{\dot{u}} \dot{u} + M_{\dot{r}} \dot{r} + M_v v + M_{\dot{v}} \dot{v}$
Pure sway	$\tilde{F}_x = X_0 + X_u u + X_r r + X_{\dot{u}} \dot{u} + X_{\dot{r}} \dot{r} + X_v v + X_{\dot{v}} \dot{v} + X_{vv} v^2$ $\tilde{F}_y = Y_0 + Y_u u + Y_r r + Y_{\dot{u}} \dot{u} + Y_{\dot{r}} \dot{r} + Y_v v + Y_{\dot{v}} \dot{v} + Y_{v\|v\|} v\|v\|$ $\tilde{M}_z = M_0 + M_u u + M_r r + M_{\dot{u}} \dot{u} + M_{\dot{r}} \dot{r} + M_v v + M_{\dot{v}} \dot{v} + M_{v\|v\|} v\|v\|$
Yaw and drift	$\tilde{F}_x = X_0 + X_u u + X_r r + X_{rr} r^2 + X_{\dot{u}} \dot{u} + X_{\dot{r}} \dot{r} + X_{\dot{v}} \dot{v} + X_v v + X_{vr} vr + X_{uu} u^2 + X_{vv} v^2 + X_{uv} uv$ $\tilde{F}_y = Y_0 + Y_u u + Y_r r + Y_{rrr} r^3 + Y_{\dot{u}} \dot{u} + Y_v v + Y_{vu} vu + Y_{v\|v\|} v\|v\| + Y_{v\|r\|} v\|r\| + Y_{r\|v\|} r\|v\| + Y_{rvv} rv^2 + Y_{vrr} vr^2$ $\tilde{M}_z = M_0 + M_u u + M_r r + M_{rrr} r^3 + M_{\dot{u}} \dot{u} + M_v v + M_{vu} vu + M_{rvv} rv^2 + M_{vrr} vr^2 + M_{v\|v\|} v\|v\| + M_{v\|r\|} v\|r\| + M_{r\|v\|} r\|v\|$

Due to the absence of data reduction equations for those variables, measured forces/moment F are approximated as a polynomial expansion model $\tilde{F}$ of thevariables.

$$F \approx \tilde{F} = \sum_k \sum_{n=0}^{J} A_{k,n} (x_k)^n \tag{A39}$$

where, $n = 0, 1, \ldots, J$; $x_k = u, v, r, \dot{u}, \dot{v}, \dot{r}$; $A_{k,n}$ is the constant coefficient of n^{th} order x_k variable which is a function of time t. The number of variables k employed and/or the highest order J of each variable varies with each force component and type of test. The polynomial model definition for all forces/moment components for all test types of the UA test cases are summarized in Table A11.

With the polynomial modelling of the measured forces or moment the uncertainties in the equation (A38) are evaluated

$$U_{F,x} = \frac{\partial F}{\partial x} U_x \approx \frac{\partial \tilde{F}}{\partial x} U_x \tag{A40}$$

The coefficients of each polynomial model are calculated with the Least-Square fitting method. In equations (A38) and (A40) the standard uncertainties U_v, $U_{\dot{v}}$, U_r, $U_{\dot{r}}$, U_u, $U_{\dot{u}}$ are identical with the uncertainties defined in (A27-A32), respectively. With respect to $U_{F,t}$, the sensitivity coefficient $\partial F / \partial t$ is calculated numerically from the measured time histories of F .

A.6. Repeatability of measurement results

The uncertainties are determined from 12 repeat tests. The datasets are spaced in time at least 12 minutes between tests to minimize flow disturbances from previous runs, while spanning over a time period, usually one day, that is large relative to time scales of the factors that influence variability of the measurements. The same model ship, PMM motion generator, load cell, and motion tracker are used for the repeat tests due to limitations of time and experiment resources. The model is not dismounted and re-installed during the repeat tests. However, the PMM motion control parameters, such as drift angle, sway crank amplitude, or maximum

heading angle settings are changed between tests. The uncertainties are computed with the standard multiple-test equation

$$U_{\bar{R}} = \frac{\mathrm{k}S_{\bar{R}}}{\sqrt{12}} \tag{A41}$$

where $R = X'$, Y', N' and the coverage factor $\mathrm{k} = 2$ to obtain the expanded uncertainty. $S_{\bar{R}}$ is the standard deviation defined as

$$S_{\bar{R}} = \left[\sum_{k=1}^{12} \frac{(R_k - \bar{R})}{11}\right]^{\frac{1}{2}} \tag{A42}$$

and

$$\bar{R} = \frac{1}{12}\sum_{k=1}^{12} R_k \tag{A43}$$

where, R_k is either X', Y', or N' of the k^{th} run, which are defined in (A2-A4) for dynamic tests and (A5-A7) for static tests, respectively.

A.7. Results

The uncertainty assessment results are presented in Table A15 for static drift tests and Tables A16-A18 for dynamic tests. Each table consists of three parts;

- DRE variables and their uncertainty contributions to the expanded uncertainty of non-dimensional forces and moment U_R (top),
- uncertainties of measured forces and moments U_F including contributions from elemental uncertainties $U_{F,x}$ (middle), and
- total uncertainties their contributions to total expanded uncertainty U_{95R} (bottom). The latter includes scaled total uncertainties in percentile of either variable magnitude or its dynamic range.

For dynamic tests the UA results only at their maximum motions are presented and compared in the tables.

Static tests From Table A15 (top) the largest bias is the carriage speed U_{U_C} and the second largest uncertainty is the measured force U_F for X', while U_F is the largest uncertainty and U_{U_C} is the second largest uncertainty for Y' and N'. The measured forces/moment bias U_F, a common large uncertainty for X', Y', N', is mainly from the uncertainty in drift angle $U_{F,\beta}$ as presented in Table A15 (middle). $U_{F,\beta}$ contributes over 90% to U_F for all cases. From Table A15 (bottom), the total uncertainty U_R contributes over 90%, and the precision limit $U_{\bar{R}}$ contributes less than 10% to U_{95R}, indicating most DRE variable results are highly repeatable. Total uncertainties U_{95R}'s are reasonably small, 1.9%, 3.4%, and 2.8% of X', Y', and N' respectively. Although the static drift tests are similar with the resistance test, a steady straight towing test, additional uncertainties from the drift angle setting associated with static drift test might explain the higher uncertainty levels. Improvements of static drift test uncertainty can be achieved by improving the carriage speed control for X' and drift angle setting accuracy for Y' and N', which are the biggest uncertainty sources.

Dynamic tests For pure yaw tests (Table A16), the primary bias is surge velocity U_u and the secondary is measured forces/moment U_F for X', U_F is the primary bias and the yaw rate U_r is secondary bias for Y', and again U_F is the primary and U_u is the secondary biases for N', respectively. The measured forces/moment bias U_F is composed largely of surge velocity $U_{F,u}$ and acceleration $U_{F,\dot{u}}$ for F_x, and of the yaw rate $U_{F,r}$ for F_y and M_z, respectively. The type B uncertainty $U_{\overline{X'}}$ is dominant (75%) for X', but the type A uncertainty $U_{Y'}$ and $U_{N'}$ are dominant (> 90%) for Y' and N'. The total uncertainty $U_{\overline{X'}}$ is 8% of X', and $U_{\overline{Y'}}$ and $U_{\overline{N'}}$ are 5%, and 1.4% of the dynamic ranges of Y' and N', respectively.

For pure sway test (Table A17), the surge velocity U_u is the primary source of uncertainty and measured force U_F and mean draft U_{T_m} are secondary source of uncertainty for X', U_F is the primary source of uncertainty and U_u is the secondary source of uncertainty for Y' and N', respectively. $U_{L_{\mathrm{PP}}}$, U_{x_G}, U_{y_G}, U_m, U_{I_z}, U_ρ, U_v, U_r, $U_{\dot{u}}$, $U_{\dot{v}}$, $U_{\dot{r}}$ all contribute small or negligibly for all cases. The measured forces/moment bias U_F is composed mainly of the sway velocity $U_{F,v}$ for all F, but also from $U_{F,\mathrm{acquis}}$ and $U_{F,u}$ for U_{F_x}. $U_{95X'}$ is 5.8% of X', and $U_{95Y'}$ and $U_{95N'}$ are all 2.1% of the dynamic ranges of Y' and N', respectively.

For yaw and drift tests (Table A18), the surge velocity U_u is the primary source of uncertainty and the measured forces/moment U_F is the secondary source of uncertainty for X', U_F is the primary and the yaw rate U_r is the secondary source of uncertainty for Y', and U_F is primary and U_u is the secondary source of uncertainty for N', respectively. The total uncertainty $U_{95X'}$ is about 7% of X', $U_{95Y'}$ and $U_{95N'}$ are 3.6% and 1.5% of the dynamic ranges of Y' and N', respectively.

In conclusion for the dynamic tests, primary source of uncertainty vary according to type of the test while the measured forces/moment source of uncertainty U_F is the common largest source of uncertainty. Ship model geometry related source of uncertainty and water density source of uncertainty are contributing small or negligibly except for the mean draft bias U_{T_m} and the longitudinal COG bias U_{x_G}. However, the uncertainties from motion parameters and measured forces/moment are dominant according to forces/moment component and test type. For the dynamic tests, the total uncertainties U_{95R}'s are varying 6% ~ 8% of X', 1% ~ 5% of Y' and N' according to test type, which are larger than those of the static drift test results. Of the four different types of dynamic PMM tests, the pure yaw test total uncertainty is relatively higher than other kinds of PMM tests. The uncertainty of the dynamic test results can be improved by improving carriage speed control and increasing the number of repeat to reduce the type B uncertainty for X', and by improving the PMM motion control to reduce type A uncertainty for Y' and N', respectively.

A.8. List of symbols

A_{WP} Water plane area
B_{WL} Breadth of water line
COG Centre of gravity
Fr Froude number
F_X, F_Y, F_Z Measured forces
I_Z Yaw moment of inertia
L_{PP} Length between perpendiculars
L_{WL} Length of water line
m Mass
M Number of repeats
M_X, M_Y, M_Z Measured moments
N Number of PMM rotations per minute
R_k X', Y' or N' of k$^{\mathrm{th}}$ repeat test
S_{mm} Sway crank amplitude
$S_{\bar{R}}$ Standard deviation of repeat tests
t Time
T_m Mean draft
u, v, r Surge, sway and yaw velocities
u', v', r' Non-dimensional surge, sway and yaw velocities
$\dot{u}, \dot{v}, \dot{r}$ Surge, sway and yaw accelerations
U_C Carriage speed
U_X Uncertainty of variable x
x, y, z Axes
x_G Longitudinal centre of gravity
y_G Transverse centre of gravity
X, Y, N Hydrodynamic forces and moments
β Drift angle
Δ Displacement mass
ε_X Uncertainty of variable x
η_{PMM} Transverse translation
θ_X Sensitivity coefficient
ρ Density of water
ψ Heading

ψ_0 Yaw motion amplitude
ω PMM frequency
∇ Displacement volume

Table A12 Definitions of sensitivity coefficients for $U_{X'}$.

	Dynamic Tests	Static Tests
θ_{F_x}	$\frac{2}{\rho(u^2+v^2)T_{\mathrm{m}}L_{\mathrm{PP}}}$	$\frac{2}{\rho U_C^2 T_{\mathrm{m}} L_{\mathrm{PP}}}$
θ_ρ	$\frac{-2\left(F_x+m\left(\dot{u}-rv-x_{\mathrm{G}}r^2-y_{\mathrm{G}}\dot{r}\right)\right)}{\rho^2(u^2+v^2)T_{\mathrm{m}}L_{\mathrm{PP}}}$	$\frac{-2F_x}{\rho^2 U_C^2 T_{\mathrm{m}} L_{\mathrm{PP}}}$
$\theta_{T_{\mathrm{m}}}$	$\frac{-2\left(F_x+m\left(\dot{u}-rv-x_{\mathrm{G}}r^2-y_{\mathrm{G}}\dot{r}\right)\right)}{\rho(u^2+v^2)T_{\mathrm{m}}^2L_{\mathrm{PP}}}$	$\frac{-2F_x}{\rho U_C^2 T_{\mathrm{m}}^2 L_{\mathrm{PP}}}$
$\theta_{L_{\mathrm{PP}}}$	$\frac{-2\left(F_x+m\left(\dot{u}-rv-x_{\mathrm{G}}r^2-y_{\mathrm{G}}\dot{r}\right)\right)}{\rho(u^2+v^2)T_{\mathrm{m}}L_{\mathrm{PP}}^2}$	$\frac{-2F_x}{\rho U_C^2 T_{\mathrm{m}} L_{\mathrm{PP}}^2}$
$\theta_{U_{\mathrm{C}}}$	-	$\frac{-4F_x}{\rho U_C^3 T_{\mathrm{m}} L_{\mathrm{PP}}}$
θ_m	$\frac{2\left(\dot{u}-rv-x_{\mathrm{G}}r^2-y_{\mathrm{G}}\dot{r}\right)}{\rho(u^2+v^2)T_{\mathrm{m}}L_{\mathrm{PP}}}$	-
θ_{x_G}	$\frac{-2mr^2}{\rho(u^2+v^2)T_{\mathrm{m}}L_{\mathrm{PP}}}$	-
θ_{y_G}	$\frac{-2m\dot{r}}{\rho(u^2+v^2)T_{\mathrm{m}}L_{\mathrm{PP}}}$	-
θ_u	$\frac{-4u\left(F_x+m\left(\dot{u}-rv-x_{\mathrm{G}}r^2-y_{\mathrm{G}}\dot{r}\right)\right)}{\rho(u^2+v^2)^2T_{\mathrm{m}}L_{\mathrm{PP}}}$	-
$\theta_{\dot{u}}$	$\frac{-2m}{\rho(u^2+v^2)T_{\mathrm{m}}L_{\mathrm{PP}}}$	-
θ_v	$\frac{2}{\rho(u^2+v^2)T_{\mathrm{m}}L_{\mathrm{PP}}}\left[-mr-\frac{2v\left(F_x+m\left(\dot{u}-rv-x_{\mathrm{G}}r^2-y_{\mathrm{G}}\dot{r}\right)\right)}{(u^2+v^2)}\right]$	-
θ_r	$\frac{-2m(v+2x_{\mathrm{G}}r)}{\rho(u^2+v^2)T_{\mathrm{m}}L_{\mathrm{PP}}}$	-
$\theta_{\dot{r}}$	$\frac{-2my_{\mathrm{G}}}{\rho(u^2+v^2)T_{\mathrm{m}}L_{\mathrm{PP}}}$	-

Table A13 Definitions of sensitivity coefficients for $U_{Y'}$.

	Dynamic Tests	Static Tests
θ_{F_y}	$\frac{2}{\rho(u^2+v^2)T_{\mathrm{m}}L_{\mathrm{PP}}}$	$\frac{2}{\rho U_C^2 T_{\mathrm{m}} L_{\mathrm{PP}}}$
θ_{ρ}	$\frac{-2\left(F_y+m\left(\dot{v}+ru-y_{\mathrm{G}}r^2+x_{\mathrm{G}}\dot{r}\right)\right)}{\rho^2(u^2+v^2)T_{\mathrm{m}}L_{\mathrm{PP}}}$	$\frac{-2F_y}{\rho^2 U_C^2 T_{\mathrm{m}} L_{\mathrm{PP}}}$
$\theta_{T_{\mathrm{m}}}$	$\frac{-2\left(F_y+m\left(\dot{v}+ru-y_{\mathrm{G}}r^2+x_{\mathrm{G}}\dot{r}\right)\right)}{\rho(u^2+v^2)T_{\mathrm{m}}^2L_{\mathrm{PP}}}$	$\frac{-2F_y}{\rho U_C^2 T_{\mathrm{m}}^2 L_{\mathrm{PP}}}$
$\theta_{L_{\mathrm{PP}}}$	$\frac{-2\left(F_y+m\left(\dot{v}+ru-y_{\mathrm{G}}r^2+x_{\mathrm{G}}\dot{r}\right)\right)}{\rho(u^2+v^2)T_{\mathrm{m}}L_{\mathrm{PP}}^2}$	$\frac{-2F_y}{\rho U_C^2 T_{\mathrm{m}} L_{\mathrm{PP}}^2}$
θ_{U_C}	-	$\frac{-4F_y}{\rho U_C^3 T_{\mathrm{m}} L_{\mathrm{PP}}}$
θ_m	$\frac{2\left(\dot{v}+ru-y_{\mathrm{G}}r^2+x_{\mathrm{G}}\dot{r}\right)}{\rho(u^2+v^2)T_{\mathrm{m}}L_{\mathrm{PP}}}$	-
$\theta_{x_{\mathrm{G}}}$	$\frac{2m\dot{r}}{\rho(u^2+v^2)T_{\mathrm{m}}L_{\mathrm{PP}}}$	-
$\theta_{y_{\mathrm{G}}}$	$\frac{-2mr^2}{\rho(u^2+v^2)T_{\mathrm{m}}L_{\mathrm{PP}}}$	-
θ_u	$\frac{2}{\rho(u^2+v^2)T_{\mathrm{m}}L_{\mathrm{PP}}}\left[mr-\frac{2u\left(F_y+m\left(\dot{v}+ru-y_{\mathrm{G}}r^2+x_{\mathrm{G}}\dot{r}\right)\right)}{(u^2+v^2)}\right]$	-
θ_v	$\frac{-4v\left(F_y+m\left(\dot{v}+ru-y_G r^2+x_G\dot{r}\right)\right)}{\rho(u^2+v^2)^2T_mL_{PP}}$	-
$\theta_{\dot{v}}$	$\frac{2m}{\rho(u^2+v^2)T_{\mathrm{m}}L_{\mathrm{PP}}}$	-
θ_r	$\frac{2m(u-2y_{\mathrm{G}}r)}{\rho(u^2+v^2)T_{\mathrm{m}}L_{\mathrm{PP}}}$	-
$\theta_{\dot{r}}$	$\frac{2mx_{\mathrm{G}}}{\rho(u^2+v^2)T_{\mathrm{m}}L_{\mathrm{PP}}}$	-

Table A14 Definitions of the sensitivity coefficients for $U_{N'}$.

	Dynamic Tests	Static Tests
θ_{M_z}	$\frac{2}{\rho(u^2+v^2)T_{\mathrm{m}}L_{\mathrm{PP}}^2}$	$\frac{2}{\rho U_{\mathrm{C}}^2 T_{\mathrm{m}} L_{\mathrm{PP}}^2}$
θ_{ρ}	$\frac{-2\left(M_z+I_z\dot{r}+m\left(x_{\mathrm{G}}(\dot{v}+ru)-y_{\mathrm{G}}(\dot{u}-rv)\right)\right)}{\rho^2(u^2+v^2)T_{\mathrm{m}}L_{\mathrm{PP}}^2}$	$\frac{-2M_z}{\rho^2 U_{\mathrm{C}}^2 T_{\mathrm{m}} L_{\mathrm{PP}}^2}$
$\theta_{T_{\mathrm{m}}}$	$\frac{-2\left(M_z+I_z\dot{r}+m\left(x_{\mathrm{G}}(\dot{v}+ru)-y_{\mathrm{G}}(\dot{u}-rv)\right)\right)}{\rho(u^2+v^2)T_{\mathrm{m}}^2L_{\mathrm{PP}}^2}$	$\frac{-2M_z}{\rho U_C^2 T_m^2 L_{PP}^2}$
$\theta_{L_{\mathrm{PP}}}$	$\frac{-4\left(M_z+I_z\dot{r}+m\left(x_{\mathrm{G}}(\dot{v}+ru)-y_{\mathrm{G}}(\dot{u}-rv)\right)\right)}{\rho(u^2+v^2)T_{\mathrm{m}}L_{\mathrm{PP}}^3}$	$\frac{-4M_z}{\rho U_C^2 T_m L_{PP}^3}$
$\theta_{U_{\mathrm{C}}}$	-	$\frac{-4M_z}{\rho U_C^3 T_m L_{PP}^2}$
θ_{I_z}	$\frac{2\dot{r}}{\rho(u^2+v^2)T_{\mathrm{m}}L_{\mathrm{PP}}^2}$	-
θ_m	$\frac{2\left(x_{\mathrm{G}}(\dot{v}+ru)-y_{\mathrm{G}}(\dot{u}-rv)\right)}{\rho(u^2+v^2)T_{\mathrm{m}}L_{\mathrm{PP}}^2}$	-
$\theta_{x_{\mathrm{G}}}$	$\frac{2m(\dot{v}+ru)}{\rho(u^2+v^2)T_{\mathrm{m}}L_{\mathrm{PP}}^2}$	-
$\theta_{y_{\mathrm{G}}}$	$\frac{-2m(\dot{u}-rv)}{\rho(u^2+v^2)T_{\mathrm{m}}L_{\mathrm{PP}}^2}$	-
θ_u	$\frac{2}{\rho(u^2+v^2)T_{\mathrm{m}}L_{\mathrm{PP}}^2}\left[mx_{\mathrm{G}}r-\frac{2u\left(M_z+I_z\dot{r}+m\left(x_{\mathrm{G}}(\dot{v}+ru)-y_{\mathrm{G}}(\dot{u}-rv)\right)\right)}{(u^2+v^2)}\right]$	-
$\theta_{\dot{u}}$	$\frac{-2my_{\mathrm{G}}}{\rho(u^2+v^2)T_{\mathrm{m}}L_{\mathrm{PP}}^2}$	-
θ_v	$\frac{2}{\rho(u^2+v^2)T_{\mathrm{m}}L_{\mathrm{PP}}^2}\left[my_{\mathrm{G}}r-\frac{2v\left(M_z+I_z\dot{r}+m\left(x_{\mathrm{G}}(\dot{v}+ru)-y_{\mathrm{G}}(\dot{u}-rv)\right)\right)}{(u^2+v^2)}\right]$	-
$\theta_{\dot{v}}$	$\frac{2mx_{\mathrm{G}}}{\rho(u^2+v^2)T_{\mathrm{m}}L_{\mathrm{PP}}^2}$	-
θ_r	$\frac{2m(x_{\mathrm{G}}u+y_{\mathrm{G}}v)}{\rho(u^2+v^2)T_{\mathrm{m}}L_{\mathrm{PP}}^2}$	-
$\theta_{\dot{r}}$	$\frac{2I_z}{\rho(u^2+v^2)T_{\mathrm{m}}L_{\mathrm{PP}}^2}$	-

Table A15 UA summary of static drift test (β = -10°).

R	Var. (x)	L_{PP}	T_m	ρ	U_C	F
	Unit	m	m	kg/m³	m/s	N,Nm
	Mag.	3.048	0.132	998.1	1.531	-
	U_x	0.002	0.001	0.041	0.011	-
X'	$\frac{\theta_x^2 U_x^2}{U_R^2}$	0.1	15.8	0.0	49.4	34.7
Y'	(%)	0.0	5.3	0.0	16.6	78.0
X'		0.1	3.2	0.0	10.1	86.6

F	$\frac{U_{F,x}^2}{U_F^2}$ (%)				U_F	$\lvert F \rvert$	$\frac{U_F}{\lvert F \rvert}$
	β	align	calib	acquis	[N]	[N]	(%)
F_x	91.8	1.7	0.0	6.5	0.122	10.9	1.1
F_y	97.0	1.8	0.0	1.2	0.826	28.5	2.9
M_z	96.8	1.8	0.1	1.4	1.118	44.1	2.5

R	U_R	$\frac{U_R^2}{U_{95R}^2}$	$U_{\bar{R}}$	$\frac{U_{\bar{R}}^2}{U_{95R}^2}$	U_{95R}	$\lvert \bar{R} \rvert$	$\frac{U_{95R}}{\lvert \bar{R} \rvert}$
	[10^{-2}]	(%)	[10^{-2}]	(%)	[10^{-2}]	[-]	(%)
X'	0.045	96.6	0.008	3.4	0.045	0.023	1.9
Y'	0.201	95.1	0.046	4.9	0.206	0.061	3.4
N'	0.085	94.5	0.020	5.5	0.087	0.031	2.8

Table A16 UA summary of pure yaw test ($r = r_{max}$).

R	Var. (x)	L_{PP}	T_m	x_G	y_G	m	I_z	ρ	u	v	r	$\dot{u}$	$\dot{v}$	$\dot{r}$	F
	Unit	m	m	m	m	kg	kgm²	kg/m³	m/s	m/s	rad/s	m/s²	m/s²	rad/s²	N,Nm
	Mag.	3.048	0.132	-0.016	0.000	82.55	49.79	998.1	1.527	0.002	0.150	0.000	0.003	0.000	-
	U_x	0.002	0.001	0.005	0.002	0.11	1.84	0.041	0.010	0.006	0.003	0.002	0.002	0.000	-
X'	$\frac{\theta_x^2 U_x^2}{U_R^2}$	0.0	4.0	0.1	0.0	0.0	-	0.0	67.6	3.7	0.0	11.0	-	0.0	13.5
Y'		0.0	0.6	0.0	0.0	0.1	-	0.0	9.0	0.0	27.1	-	3.2	0.0	60.0
N'	(%)	0.0	8.1	3.3	0.0	0.0	0.0	0.0	24.8	0.0	0.0	0.0	0.0	0.0	63.5

F	r_{max}	$\frac{U_{F,x}^2}{U_F^2}$ (%)									U_F	F	$\frac{U_F}{\lvert F \rvert}$	D_F†	$\frac{U_F}{D_F}$
	[rad/s]	calib	acquis	u	v	r	$\dot{u}$	$\dot{v}$	$\dot{r}$	t	[N] [Nm]	[N] [Nm]	(%)	[N] [Nm]	(%)
F_x		0.0	4.3	11.5	0.0	4.0	55.1	25.0	0.0	0.1	0.140	-10.06	1.4	-	-
F_y	0.150	0.0	2.1	7.1	0.0	89.8	0.0	1.0	0.0	0.0	0.606	-27.27	2.2	54.36	1.1
M_z		0.4	2.0	0.8	0.0	95.8	0.1	0.9	0.0	0.0	0.457	-21.26	2.1	47.67	1.0

R	r_{max}	U_R	$\frac{U_R^2}{U_{95R}^2}$	$U_{\bar{R}}$	$\frac{U_{\bar{R}}^2}{U_{95R}^2}$	U_{95R}	$\bar{R}$	$\frac{U_{95R}}{\lvert \bar{R} \rvert}$	D_R†	$\frac{U_{95R}}{D_R}$
	[rad/s]	[10^{-2}]	(%)	[10^{-2}]	(%)	[10^{-2}]	[-]	(%)	[-]	(%)
X'		0.081	24.7	0.142	75.3	0.163	-0.021	7.6	-	-
Y'	0.150	0.167	94.2	0.042	5.8	0.172	-0.017	10.0	0.034	5.0
N'		0.040	90.0	0.013	10.0	0.042	-0.015	2.8	0.031	1.4

† D: Dynamic range of the variable $D = \lvert max - min \rvert$

Table A17 UA summary of pure sway test ($v = v_{\max}$).

R	Var. (x)	L_{PP}	T_m	x_G	y_G	m	I_z	ρ	u	v	r	$\dot{u}$	$\dot{v}$	$\dot{r}$	F
	Unit	m	m	m	m	kg	kgm²	kg/m³	m/s	m/s	rad/s	m/s²	m/s²	rad/s²	N,Nm
	Mag.	3.048	0.132	-0.016	0.000	82.55	49.79	998.1	1.518	0.269	0.000	0.000	0.001	-0.001	-
	U_x	0.002	0.001	0.005	0.002	0.11	1.84	0.041	0.010	0.008	0.000	0.000	0.000	0.000	-
X'	$\frac{\theta_x^2 U_x^2}{U_R^2}$	0.0	4.9	0.0	0.0	0.0	-	0.0	82.8	0.3	-	0.0	-	0.0	12.0
Y'		0.0	3.2	0.0	0.0	0.0	-	0.0	9.5	1.1	0.0	-	0.0	0.0	86.1
N'	(%)	0.1	3.5	0.0	0.0	0.0	0.0	0.0	10.5	0.2	0.0	0.0	0.0	0.5	85.2

F	$v_{\max}$	$\frac{U_{F,x}^2}{U_F^2}$ (%)									U_F	F	$\frac{U_F}{\lvert F\rvert}$	D_F†	$\frac{U_F}{D_F}$
	[m/s]	calib	acquis	u	v	r	$\dot{u}$	$\dot{v}$	$\dot{r}$	t	[N] [Nm]	[N] [Nm]	(%)	[N] [Nm]	(%)
F_x		0.0	5.6	8.9	85.5	0.0	0.0	0.0	0.0	0.0	0.166	-13.91	1.2	-	-
F_y	0.269	0.0	0.7	0.0	99.2	0.0	0.0	0.1	0.0	0.0	1.168	-29.55	4.0	86.08	1.4
M_z		0.0	0.6	0.0	99.3	0.0	0.0	0.0	0.0	0.0	1.770	-47.10	3.8	94.46	1.9

R	$v_{\max}$	U_R	$\frac{U_R^2}{U_{95R}^2}$	$U_{\bar{R}}$	$\frac{U_{\bar{R}}^2}{U_{95R}^2}$	U_{95R}	$\bar{R}$	$\frac{U_{95R}}{\lvert\bar{R}\rvert}$	D_R†	$\frac{U_{95R}}{D_R}$
	[m/s]	[10^{-2}]	(%)	[10^{-2}]	(%)	[10^{-2}]	[-]	(%)	[-]	(%)
X'		0.100	35.4	0.135	64.6	0.168	-0.029	5.8	-	-
Y'	0.269	0.264	91.2	0.082	8.8	0.276	-0.062	4.5	0.133	2.1
N'		0.132	97.7	0.020	2.3	0.133	-0.032	4.1	0.065	2.1

† D: Dynamic range of the variable $D = |max - min|$

Table A18 UA summary of yaw and drift test ($r = r_{\max}$).

R	Var. (x)	L_{PP}	T_m	x_G	y_G	m	I_z	ρ	u	v	r	$\dot{u}$	$\dot{v}$	$\dot{r}$	F
	Unit	m	m	m	m	kg	kgm²	kg/m³	m/s	m/s	rad/s	m/s²	m/s²	rad/s²	N,Nm
	Mag.	3.048	0.132	-0.016	0.000	82.55	49.79	998.1	1.503	-0.263	0.151	0.001	0.004	0.000	-
	U_x	0.002	0.001	0.005	0.002	0.11	1.84	0.041	0.010	0.006	0.003	0.002	0.002	0.000	-
X'	$\frac{\theta_x^2 U_x^2}{U_R^2}$	0.0	3.8	0.0	0.0	0.0	-	0.0	60.2	1.5	2.2	8.8	-	0.0	23.5
Y'		0.0	2.8	0.0	0.0	0.1	-	0.0	2.6	0.5	16.1	-	2.0	0.0	76.0
N'	(%)	0.1	2.4	1.2	0.0	0.0	0.0	0.0	7.1	0.1	0.0	0.0	0.0	0.0	89.2

F	$r_{\max}$	$\frac{U_{F,x}^2}{U_F^2}$ (%)									U_F	F	$\frac{U_F}{\lvert F\rvert}$	D_F†	$\frac{U_F}{D_F}$
	[rad/s]	calib	acquis	u	v	r	$\dot{u}$	$\dot{v}$	$\dot{r}$	t	[N] [Nm]	[N] [Nm]	(%)	[N] [Nm]	(%)
F_x		0.0	3.5	36.6	0.4	31.5	26.9	1.1	0.0	0.0	0.235	-15.78	1.5	-	-
F_y	0.151	0.0	0.0	13.3	36.7	45.8	0.3	3.9	0.0	0.0	0.872	2.94	29.7	67.48	1.3
M_z		0.1	0.4	1.8	53.0	38.5	0.2	5.9	0.1	0.0	0.896	19.54	4.6	66.37	1.4

R	$r_{\max}$	U_R	$\frac{U_R^2}{U_{95R}^2}$	$U_{\bar{R}}$	$\frac{U_{\bar{R}}^2}{U_{95R}^2}$	U_{95R}	$\bar{R}$	$\frac{U_R}{\lvert\bar{R}\rvert}$	D_R†	$\frac{U_{95R}}{D_R}$
	[rad/s]	[10^{-2}]	(%)	[10^{-2}]	(%)	[10^{-2}]	[-]	(%)	[-]	(%)
X'		0.104	32.9	0.148	67.1	0.181	-0.027	6.8	-	-
Y'	0.151	0.214	82.4	0.099	17.6	0.236	0.047	5.0	0.065	3.6
N'		0.067	93.2	0.018	6.8	0.069	0.014	5.1	0.045	1.5

† D: Dynamic range of the variable $D = |max - min|$

Appendix B.
MEAN DRAFT UNCERTAINTY U_{TM}

If the model ship is ballasted based on displacement, U_{T_m} is composed of two uncorrelated elemental uncertainties, $U_{T_m,d1}$ from the model manufacturing and $U_{T_m,d2}$ from the uncertainty related to ballast weights. By assuming the model uncertainty to be ±1mm in all coordinates, as given in ITTC Procedure 7.5-01-01-01, 'Ship Models', and these dimensions are changed while keeping the block coefficient constant, the uncertainty in the displacement of the model can be calculated using

$$\nabla' = \rho(L_{PP} + \varepsilon_L)(B + \varepsilon_B)(T + \varepsilon_T) \qquad \text{(B1)}$$

where, ρ is the water density, L, B, T are model length, beam, draft, respectively, and ε_L = 2 mm, ε_B = 2 mm, ε_T = 1 mm are uncertainties in length, beam, draft, respectively. Then $U_{T_m,d1}$ can be estimated as

$$U_{T_m,d1} = \frac{\nabla' - \nabla}{\rho A_{WP}} = 0.0011\ \text{m} \qquad \text{(B2)}$$

where A_{WP} is the water plane area of the model given in Table A1. $U_{T_m,d2}$ can be estimated from the total mass bias U_m by equating with the displacement change

$$U_{T_m,d2} = \frac{U_m}{\rho A_{WP}} = 0.0001\ \text{m} \qquad \text{(B3)}$$

Then, U_{T_m} = 0.001 m is estimated as the RSS of $U_{T_m,d1}$ and $U_{T_m,d2}$.

B.1. List of symbols

A_{WP}	Water plane area
B	Beam
L_{PP}	Model length
T_m	Mean draft
ε_X	Uncertainty of variable x
ρ	Density of water
∇	Displacement volume

Appendix C.
MOMENT OF INERTIA UNCERTAINTY U_{IZ}

Generally, yaw moment of inertia can be measured by measuring yawing periods T while swinging a given mass attached to, for example, a steel rod with known torsion stiffness G (*swinging method*), or by measuring the yaw moment while enforcing a sinusoidal yaw motion to the mass (*yawing method*).

If the *swinging method* is used, the moment of inertia of the mass is

$$I_z = GgT^2 \tag{C1}$$

where g is the gravitational acceleration. The uncertainty of the measured I_z can be estimated as:

$$U_{I_z}^2 = \theta_G^2 U_G^2 + \theta_T^2 U_T^2 \tag{C2}$$

where, sensitivity coefficients are calculated by differentiating equation (C1) with respect to each variable. The uncertainties U_G and U_T should be estimated according to their test procedures used. Details of this method are provided by Simonsen (2004).

If the *yawing method* is used, the moment of inertia of the mass is determined from the motion equation of simple yaw:

$$-M_z = I_z \ddot{\psi} \tag{C3}$$

where, $\psi = -\psi_o \cos\omega t$ and M_z is the moment measured during the applied yaw motion. The measured moment can be represented by a Fourier series with the applied yaw motion frequency ω as the base frequency:

$$I_z = \frac{M_z^{FSC1}}{\psi_0 \omega^2} \tag{C4}$$

where, M_z^{FSC1} is the 1st harmonic amplitude of measured yaw moment, ψ_0 is the applied yaw motion amplitude, and $\omega = 2\pi N/60$ is the yaw motion frequency, N being the number of cycles per minute.

$$M_z^{FSC1} = \frac{2}{J} \sum_{j=1}^{J} M_{z_j} \cos\omega t_j \tag{C5}$$

If multiple measurements with combinations of different ψ_0's and ω's are conducted, the yaw moment of inertia can be determined with a least-square (LS) regression method.

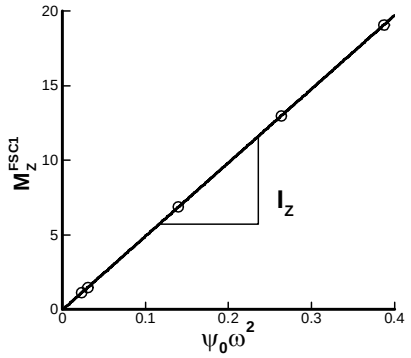

Figure C1. Relationship between the yaw moment and the vertical moment of inertia

Hence the uncertainty of the measured yaw moment of inertia U_{I_z} is considered as the RSS of each uncertainty of individual measurement $U_{I_z,i}$ and the uncertainty related to least squaring which is $U_{I_z,LS}$:

$$U_{I_z}^2 = \sum_i U_{I_z,i}^2 + U_{I_z,LS}^2 \tag{C6}$$

$U_{I_z,i}$ in equation (C6) can be defined as

$$U_{I_z,i}^2 = \theta_{M_{z,i}^{FSC1}}^2 U_{M_{z,i}^{FSC1}}^2 + \theta_{\psi_0,i}^2 U_{\psi_0,i}^2 + \theta_{\omega,i}^2 U_{\omega,i}^2 \tag{C7}$$

Sensitivity coefficients are calculated analytically from the equation (C6). $U_{M_{z,i}^{FSC1}}$ is defined from equation (C5),

$$U^2_{M^{FSC1}_{z,i}} = \sum_{j=1}^{J} \theta^2_{M_{z,i_j}} U^2_{M_{z,i_j}} + \theta^2_{\omega_i} U^2_{\omega_i} + \sum_{j=1}^{J} \theta^2_{t_j} U^2_{t_j} \quad \text{(C8)}$$

where, $U_{\omega_i} = 2\pi U_N / 60$. $U_{M_{z_j}}$ is estimated as 3% of $U_{M_z^{FSC1}}$. Finally $U_{I_z,LS}$ is quantified with the standard estimate of error (SEE) from Coleman and Steel (1999),

$$U_{I_z,LS} = \sqrt{\sum_{i=1}^{L} \frac{(I_z - I_{z,i})^2}{L-1}} \quad \text{(C9)}$$

where, I_z is the least squared regression result and $I_{z,i}$ is the result of individual measurements.

If the yaw moment of inertia of the model ship is measured together with a mount or a yoke to hold the model ship, and if part of ballasting weights is added or removed while mounting, the yaw moment of inertia of the model is

$$I_z = I_{z,\text{Total}} - I_{z,\text{mount}} \pm \sum_k I_{z,\text{ballast},k} \quad \text{(C10)}$$

where, I_z is the moment of inertia of the model, $I_{z,\text{Total}}$ is the total moment of inertia of combined model and mount or yoke, $I_{z,\text{mount}}$ is that of the mount or yoke, and $I_{z,\text{ballast},k}$ is the moment of inertia of the ballast weights added or excluded. If the moment of inertia of each ballast weight with respect to its own axis and the distance to the midship are known, the moment of inertia of the ballast weight is calculated by using the parallel axis theorem

$$\sum_k I_{z,\text{ballast},k} = \sum_k \left(I_{z,\text{own},k} + r_k^2 m_k \right) \quad \text{(C11)}$$

where r_k is the distance to the midship and m_k is the weight of the ballast weight. By applying the uncertainty propagation equation to equation (C11), $U_{I_z,\text{ballast},k}$ is

$$U^2_{I_z,\text{ballast},k} = \theta^2_{I_z,\text{own},k} U^2_{I_z,\text{own},k} + \theta^2_{r_k} U^2_{r_k} + \\ + \theta^2_{m_k} U^2_{m_k} \quad \text{(C12)}$$

Then U_{I_z} is

$$U^2_{I_z} = U^2_{I_z,\text{Total}} + U^2_{I_z,\text{mount}} + \sum_k U^2_{I_z,\text{ballast},k} \quad \text{(C13)}$$

$U_{I_z,\text{Total}}$ and $U_{I_z,\text{mount}}$ can be estimated either from equation (C1) or (C6) according to I_z measurement method used, and $U_{I_z,\text{ballast},k}$ can be estimated from equation (C11), respectively. An example with yawing method is presented in Table C1.

C.1. List of symbols

g	Gravitational acceleration
G	Torsion stiffness
I_Z	Yaw moment of inertia
m_k	Weight of ballast weight k
M_Z	Measured moment in z
N	Number of cycles per minute
r_k	Distance to amidships
t	Time
T	Yawing period
U_X	Uncertainty of variable x
θ_X	Sensitivity coefficient
ψ	Yaw motion
ψ_0	Yaw motion amplitude
ω	Frequency

C.2. References

Coleman, H. W. and Steel, W. G., 1999, “Experimentation and Uncertainty Analysis for Engineers,” Wiley & Sons.

Table C1. Moment of inertia uncertainty U_{I_z} estimation.

	i	ψ_0	f	$M_{z,i}^{FSC1}$	$I_{z,i}$	$\theta^2_{M_{z,i}^{FSC1}} U^2_{M_{z,i}^{FSC1}}$	$\theta^2_{\psi_0,i} U^2_{\psi_0,i}$	$\theta^2_{\omega,i} U^2_{\omega,i}$	$U_{I_z,i}$	$I_z - I_{z,i}$
		[deg]	[Hz]	[Nm]	[kgm^2]	[kgm^2]	[kgm^2]	[kgm^2]	[kgm^2]	[kgm^2]
Model + Mount	1	9.0	0.15	6.86	49.19	1.01E-03	1.45E+00	4.30E-05	1.20	5.16E-02
	2	17.0	0.15	12.98	49.24	1.31E-02	4.06E-01	4.31E-05	0.65	2.69E-03
	3	9.0	0.25	19.07	49.19	7.07E-02	1.45E+00	1.55E-05	1.23	5.05E-02
	$U_{I_z}^2 = \sum_i^L U_{I_z,i}^2 + \left(2\sqrt{\sum_i^L \frac{(I_z - I_{z,i})^2}{L-2}}\right)^2$; $I_{z,\text{Total}}$=49.19kgm^2 , $U_{I_{z,\text{Total}}}$= 1.84kgm^2									
Mount	1	9.0	0.15	0.15	1.05	7.67E-10	6.61E-04	1.97E-08	0.03	4.89E-02
	2	17.0	0.15	0.28	1.08	5.89E-09	1.95E-04	2.07E-08	0.01	2.23E-02
	3	9.0	0.25	0.42	1.08	1.92E-08	7.01E-04	7.51E-09	0.03	1.76E-02
	$I_{z,\text{mount}}$=1.10 kgm^2 , $U_{I_{z,\text{mount}}}$= 0.12 kgm^2									
	k	Item			$I_{z,\text{own},k}$ [kgm^2]	$\varepsilon_{I_{z,\text{own},k}}$ [kgm^2]	m_k [kg]	ε_{m_k} [kg]	r_k [m]	ε_{r_k} [m]	$U_{I_{z,\text{own},k}}$ [kgm^2]
Ballast Weights	1	Part 1			0.0014	0.00006	1.109	0.02	0.0	0.001	0.00006
	2	Part 2			0.0014	0.00006	1.109	0.02	0.75	0.001	0.01137
	3	Part 3			0.0014	0.00006	1.109	0.02	0.75	0.001	0.01137
	4	weight 1			0.0257	0.00047	2.285	0.04	0.118	0.001	0.00091
	5	weights 6, 11, 12, 13			0.0726	0.00080	9.122	0.08	0.211	0.001	0.00531
	$I_{z,\text{ballast}} = \sum_k \left(I_{z,\text{own},k} + r_k^2 m_k\right)$ $U^2_{I_{z,\text{ballast}}} = \sum_k U^2_{I_{z,\text{ballast},k}}$, $U^2_{I_{z,\text{ballast},k}} = \theta^2_{I_{z,\text{own},k}} U^2_{I_{z,\text{own},k}} + \theta^2_{r_k} \varepsilon^2_{r_k} + \theta^2_{m_k} \varepsilon^2_{m_k}$ $I_{z,\text{ballast}}$=1.70kgm^2 , $U_{I_{z,\text{ballast}}}$= 0.017kgm^2									
Model	$I_z = I_{z,\text{Total}} - I_{z,\text{mount}} + I_{z,\text{ballast}}$= 49.79kgm^2 $U_{I_z} = \sqrt{U_{I_z}^2 + U_{I_{z,\text{mount}}}^2 + U_{I_{z,\text{ballast}}}^2}$ = 1.84kgm^2									

Appendix D.
CARRIAGE SPEED UNCERTAINTY U_{U_C}

Carriage speed bias limit U_{U_C} is estimated end to end by calibrating the carriage speed with respect to reference speeds. Reference speeds are obtained by measuring travel time Δt for a known distance ΔL.

$$U_{\text{ref}} = \frac{\Delta L}{\Delta t} \quad \text{(D1)}$$

U_{U_C} is composed of two uncorrelated elemental uncertainties; the calibration uncertainty $U_{U_C,\text{calib}}$ and the data-acquisition uncertainty $U_{U_C,\text{acquis}}$,

$$U_{U_C}^2 = U_{U_C,\text{calib}}^2 + U_{U_C,\text{acquis}}^2 \quad \text{(D2)}$$

where, $U_{U_C,\text{calib}}$ is the RSS of the individual reference speed calibrations,

$$U_{U_{C,calib}} = \sqrt{\sum_i \left(\theta_{\Delta L_i}^2 U_{\Delta L_i}^2 + \theta_{\Delta t_i}^2 U_{\Delta t_i}^2\right)^2} \quad \text{(D3)}$$

where, $U_{\Delta L}$ and $U_{\Delta t}$ are the uncertainties of ΔL and Δt, respectively. $U_{U_C,\text{acquis}}$ is quantified with the standard estimate of error (SEE) as per ITTC guidelines

$$U_{U_C,\text{acquis}} = 2SEE = 2\sqrt{\sum_i^N \frac{\left(U_{C,i} - U_{\text{ref},i}\right)^2}{N-2}} \quad \text{(D4)}$$

The carriage speed measurement results are summarized in Table D1.

Table D1. Carriage speed uncertainty U_{U_C}. used in this example

i	ΔL_i [m]	Δt_i [s]	$U_{\text{ref},i}$ [m/s]	$U_{C,i}$ [m/s]	$U_{U_C,\text{calib},i}$ [m/s]
1	24.088	30.6301	0.7864	0.7840	0.000163
2	24.088	30.6985	0.7847	0.7823	0.000163
3	24.088	30.7130	0.7843	0.7816	0.000163
4	14.989	11.5026	1.5639	1.5601	0.000435
5	14.989	11.5102	1.5629	1.5590	0.000435
6	14.989	11.5204	1.5615	1.5576	0.000434
7	14.989	4.9269	2.2694	2.2631	0.000631
8	14.989	4.9315	2.2681	2.2619	0.000631
9	14.989	4.9273	2.2693	2.2629	0.000631

$U_{\Delta L}$=0.005m, $U_{\Delta t}$=0.0001sec

$U_{U_C,\text{calib}} = \sqrt{\sum_i \left(\theta_{\Delta L_i}^2 U_{\Delta L_i}^2 + \theta_{\Delta t_i}^2 U_{\Delta t_i}^2\right)^2}$ = 0.0014m/s

$U_{U_C,\text{acquis}} = 2\sqrt{\sum_i^N \frac{\left(U_{C,i} - U_{\text{ref},i}\right)^2}{N-2}}$ = 0.0102m/s

$U_{U_C} = \sqrt{U_{U_C,\text{calib}}^2 + U_{U_C,\text{acquis}}^2}$ = 0.0102m/s

D.1. List of symbols

N	Number of repeats
U_X	Uncertainty of variable x
ΔL	Reference distance
Δt	Measured travel time
θ_X	Sensitivity coefficient

Appendix E.
DRIFT ANGLE UNCERTAINTY $U_{ß}$

The uncertainty of the drift angle U_β is composed of two uncorrelated uncertainties $U_{\beta,\text{align}}$ and $U_{\beta,\text{drift}}$.

$$U_\beta = \sqrt{U_{\beta,\text{align}}^2 + U_{\beta,\text{drift}}^2} \quad \text{(E1)}$$

$U_{\beta,\text{align}}$ is the model installation uncertainty with respect to straight towing direction and assumed to be 0.03°.

$U_{\beta,\text{drift}}$ is the deviation from the drift angle setting and it is estimated end to end by calibrating the drift angle with respect to reference angles. Reference angle is achieved by measuring the chord length of the arc swept by a fixed position on the model ship due to drift angle setting.

$$\beta_{\text{ref}} = \cos^{-1}\left(1 - \frac{C^2}{2R^2}\right) \quad \text{(E2)}$$

The concept of reference angle measurement is illustrated as

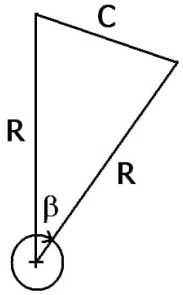

Figure E1 Concept of reference angle measurement

where, C is the chord length measured, R is the distance between midship and the measurement position. Then $U_{\beta,\text{drift}}$ can be further decomposed into two uncorrelated uncertainties $U_{\beta,\text{calib}}$ and $U_{\beta,\text{acquis}}$. The procedure to estimate these uncertainties is similar with U_{U_C} estimation. $U_{\beta,\text{drift}}$ measurement results are summarized in Table E1. Finally, U_β =0.22° is estimated from the RSS of $U_{\beta,\text{align}}$ and $U_{\beta,\text{drift}}$.

Table E1. Uncertainty in the drift angle.

i	R_i [m]	C_i [m]	$\beta_{\text{ref},i}$ [deg]	β_i [deg]	$U_{\beta,\text{calib},i}$ [deg]
1	1.998	0.068	1.96	2.00	0.00050
2	1.998	0.137	3.94	4.00	0.00050
3	1.998	0.207	5.94	6.00	0.00050
4	1.998	0.276	4.93	8.00	0.00050
5	1.998	0.344	9.87	10.00	0.00050
6	1.998	0.414	11.88	12.00	0.00051
7	1.998	-0.067	-1.93	-2.00	0.00050
8	1.998	-0.137	-3.92	-4.00	0.00050
9	1.998	-0.206	-5.92	-6.00	0.00050
10	1.998	-0.275	-4.88	-8.00	0.00050
11	1.998	-0.343	-9.84	-10.00	0.00050
12	1.998	-0.413	-11.86	-12.00	0.00051

$\beta_{\text{ref},i} = \cos^{-1}\left(1 - \frac{C^2}{2R^2}\right)$; $\varepsilon_R = \varepsilon_C = 0.001\text{m}$

$U_{\beta,\text{calib},i} = \sqrt{\theta_{R_i}^2 \varepsilon_R^2 + \theta_{C_i}^2 \varepsilon_C^2}$

$U_{\beta,\text{calib}} = \sqrt{\sum_i U_{\beta,\text{calib},i}^2} = 0.002°$

$U_{\beta,\text{acquis}} = 2\sqrt{\sum_i^N \frac{(\beta_i - \beta_{\text{ref},i})^2}{N-2}} = 0.222°$

$U_{\beta,\text{drift}} = \sqrt{U_{\beta,\text{calib}}^2 + U_{\beta,\text{acquis}}^2} = 0.222°$

E.1. List of symbols

C	Measured chord length
N	Total number of measurements
R	Distance from midship to measurement
U_X	Uncertainty of variable x
β	Drift angle
ε_X	Uncertainty of variable x

Appendix F.
EXAMPLE OF UNCERTAINTY OF THE MATHEMATICAL MANOEUVRING MODEL SIMULATED ON TURNING CHARACTERISTICS

F.1. Dataset

F.1.1. KCS in shallow water

This example, developed by the 28th Manoeuvring Committee, is based on the captive model test results of the KCS at 20% under keel clearance, carried out by Flanders Hydraulics Research (FHR) in the frame of SIMMAN 2014. The used model scale is 1/52.667. From these tests only the results at the largest velocity were selected (9 knots full scale) and from repeated tests, the average values are taken.

F.1.2. Assumptions

In this example it is assumed that all measurements are perfectly performed, the uncertainties are solely due to the data fitting. However, a change of one coefficient will affect any other coefficients due to their correlation. This correlation is neglected for reasons of simplicity but should be kept in mind. However, these assumptions do not change the methodology and if previous measurement uncertainties are known they can be added to the data fitting uncertainty.

Results are expressed in a ship fixed coordinate system. The origin is at the intersection of the midship plane, centre plane, and water plane. The x, y, z axes are directed upstream, transversely to starboard, and downward, respectively.

The presented method has been presented in literature, among others, by Woodward (2013, 2014).

F.2. Manoeuvring model

F.2.1. Formulation

For the sake of simplicity, a simple linear manoeuvring model is chosen to perform the data-fitting uncertainty analysis:

$$(Y_{\dot{v}} - m)\dot{v} + (Y_{\dot{r}} - mx_G)\dot{r} + Y_{uv}uv + (Y_{ur} - m)ur + Y_{uu\delta}uu\delta = 0 \quad \text{(F1)}$$

$$(N_{\dot{v}} - mx_G)\dot{v} + (N_{\dot{r}} - I_{ZZ})\dot{r} + N_{uv}uv + (N_{ur} - mx_G)ur + N_{uu\delta}uu\delta = 0 \quad \text{(F2)}$$

In steady state the equations simplify to

$$Y_{uv}uv + (Y_{ur} - m)ur + Y_{uu\delta}uu\delta = 0 \quad \text{(F3)}$$

$$N_{uv}uv + (N_{ur} - mx_G)ur + N_{uu\delta}uu\delta = 0 \quad \text{(F4)}$$

The dimensions of these coefficients are:

$Y_{uv}, Y_{uu\delta}$ [kg/m]
$Y_{ur}, N_{uv}, N_{uu\delta}$ [kg]
N_{ur} [kgm]

The steady state solution can be divided by $u \neq 0$:

$$Y_{uv}v + (Y_{ur} - m)r = -Y_{uu\delta}u\delta \quad \text{(F5)}$$

$$N_{uv}v + (N_{ur} - mx_G)r = -N_{uu\delta}u\delta \quad \text{(F6)}$$

Solving this set of equations to the sway and yaw velocity yields:

$$\frac{v}{u} = \frac{-Y_{uu\delta}(N_{ur} - mx_G) + N_{uu\delta}(Y_{ur} - m)}{Y_{uv}(N_{ur} - mx_G) - N_{uv}(Y_{ur} - m)}\delta \; [rad] \quad \text{(F7)}$$

$$\frac{r}{u} = \frac{Y_{uu\delta}N_{uv} - N_{uu\delta}Y_{uv}}{Y_{uv}(N_{ur} - mx_G) - N_{uv}(Y_{ur} - m)}\delta \; [rad/m] \quad \text{(F8)}$$

In case of small drift angles (linear assumptions), this leads to:

$$R \approx \frac{u}{r} = \frac{Y_{uv}(N_{ur}-mx_G)-N_{uv}(Y_{ur}-m)}{Y_{uu\delta}N_{uv}-N_{uu\delta}Y_{uv}}\frac{1}{\delta} \quad [m/rad] \tag{F9}$$

with R as steady turning radius and

$$\beta \approx -\frac{v}{u} = -\frac{-Y_{uu\delta}(N_{ur}-mx_G)+N_{uu\delta}(Y_{ur}-m)}{Y_{uv}(N_{ur}-mx_G)-N_{uv}(Y_{ur}-m)}\delta \quad [rad] \tag{F10}$$

as drift angle.

In other words an analytic solution is obtained, which makes the evaluation less difficult for a better understanding of the methodology.

F.2.2. Value of the coefficients

The application of a least square method leads to the values of the coefficients (3 significant digits) mentioned in Tables F1 and F2, in which U_{fit} represents the data-fitting uncertainty, which corresponds to the standard deviation of each coefficient.

Figure F1 and Figure F2 show the acceptable correlation of the linear model for both the sway force and the yaw moment. The linear manoeuvring model has a sufficiently acceptable prediction.

Table F1. Coefficients for steady state terms.

Derivative	Fitted value	U_{fit}	$\%U_{fit}$
$Y_{uu\delta}$	30.164	1.250	4.15
Y_{uv}	-634.522	9.399	1.48
$Y_{ur}-m$	-233.769	14.308	6.12
$N_{uu\delta}$	-52.809	1.985	3.76
N_{uv}	-897.723	14.924	1.66
$N_{ur}-mx_G$	-783.173	22.719	2.90

Table F2. Coefficients for transient terms.

Derivative	Fitted value	U_{fit}	$\%U_{fit}$
$Y_{\dot{v}}-m$	-1156.908	27.103	2.34
$Y_{\dot{r}}-mx_G$	-175.764	54.498	31.01
$N_{\dot{v}}-mx_G$	360.132	43.035	11.95
$N_{\dot{r}}-I_{ZZ}$	-1226.131	86.533	7.51

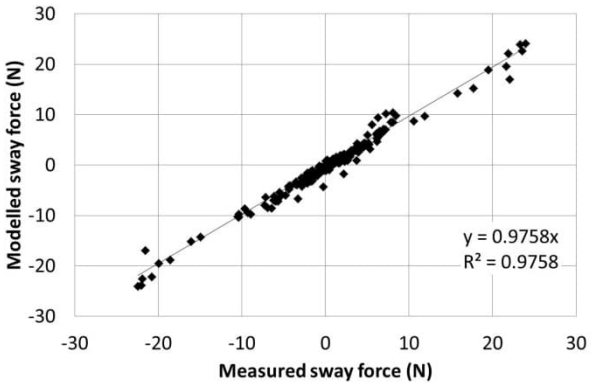

Figure F1: Modelled versus measured sway force

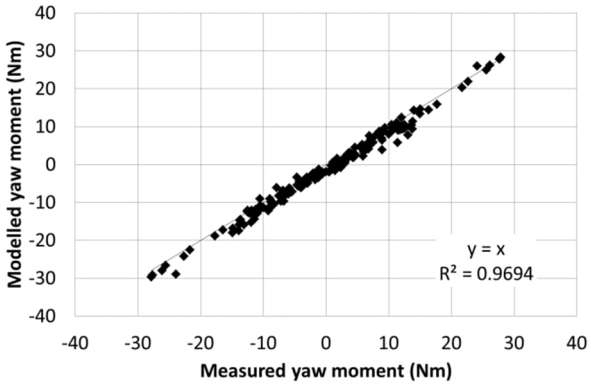

Figure F2: Modelled versus measured yaw moment

F.3. Monte Carlo Simulations

F.3.1. Methodology

The Monte Carlo simulations here are restricted to the steady turning diameter and the

drift angle while turning. In this way the simulations are reduced to a finite number of evaluations of equations (F9) and (F10). Assuming a normal probability distribution the coefficients in Table F1 can be varied between $\mu \pm 2\sigma$. This leads to a confidence interval of 95%, with:

- μ, the mean of the distribution, in this case the fitted value
- σ, the standard deviation of the distribution, in this case U_{fit}

The number of computations depends on the number of variations or steps. Two different options are considered.

F.3.2. Comprehensive assessment

The cumulative probability distribution function of the normal distribution or error function can be split in 49 steps of 2% probability, see Figure F3.

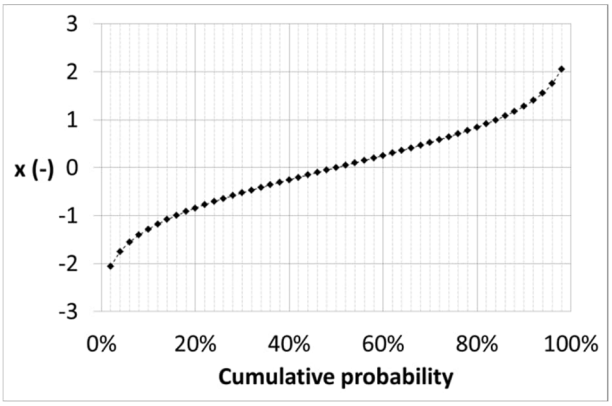

Figure F3: probability that a value is smaller than μ +x σ.

This yields 49 conditions. Each coefficient can thus have one of these 49 values. The number of possible combinations is already 49^6 or $\pm 1.4\times10^{10}$. With a computer program the steady turning radius and the drift angle have been computed for all these conditions. For a PC in 2016 the duration of all computations takes an hour.

From all computations the average and standard deviation are computed, based on the assumption that the simulation outcome is normally distributed. The latter is not always the case (see Section F.5 further in this Appendix). In the present example this yields (rounded to 3 significant digits) the values mentioned in Table F3.

Table F3. Comprehensive computation of the turning characteristics.

Parameter	Fitted value	U_{fit}	$\%U_{fit}$
$R\delta$	-4.742	0.342	7.21
β / δ	-0.126	0.010	7.88

At a rudder angle of -20° (to starboard) the vessel will have a turning diameter D of (assuming a confidence interval of 95%):

$$D = 2R = 2\left[\frac{-4.742}{rad(-20)} \pm 2\left|\frac{0.342}{rad(-20)}\right|\right] \qquad \text{(F11)}$$

Or, expressed as a function of the ship's length and only showing the significant digits:

$$D \approx -6.3 \pm 0.9L_{PP} \qquad \text{(F12)}$$

At the same time the ship will have a drift angle of (95% confidence interval):

$$\beta = -0.126(-20) \pm 2|0.01(-20)| = -2.52° \pm 0.4° \qquad \text{(F13)}$$

F.3.3. Simplified assessment

It is obvious that the number of computations or samples mc^s and consequent duration will become excessively with increasing number of steps s and model coefficients mc. A more advanced, but still simple model, e.g. of Abkowitz type has 30 coefficients, which with unchanged step size will generate a massive $\pm 5\times10^{50}$ conditions to be simulated this time.

Here a more simplified assessment is presented. A weight factor can be introduced based on the characteristics of the (normal) probability distribution. The determination of this weight factor is based on the probability of a certain value in the normal distribution, see Table F4 and Figure F4.

Table F4. Determination of the weight factor.

	$\mu \pm 0\sigma$	$\mu \pm 1\sigma$	$\mu \pm 2\sigma$
Probability	1.76%	1.07%	0.24%
Normalized	100%	60.65%	13.53%
Weight factor	10	6	1

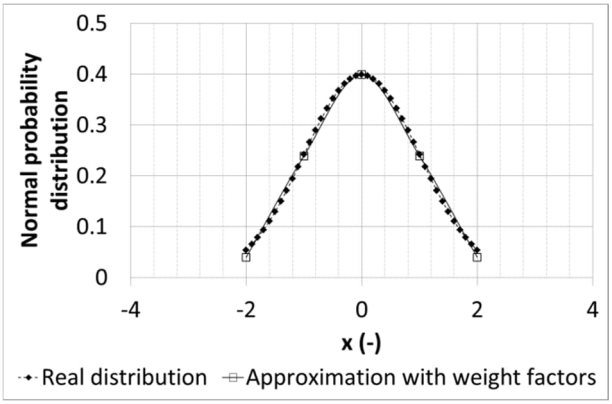

Figure F4: approximated normal probability distribution (μ = 0, σ = 1) with weight factors.

The weight factor allows to mimic the error function with a limited number of values; however these values need to be weighted according to their probability.

In essence it is still needed to consider multiple combinations, but some combinations are repeated, hence further reducing the number of needed simulations. In this simple example such reduction was not considered. 24 conditions were considered, which corresponds to the sum of the weight factors. The maximal number of combinations is 24^6 or $\pm 2\times 10^8$. For a PC in 2016 the duration of all computations takes a minute. The result is shown in Table F5.

Table F5. Simplified computation of the turning characteristics.

Parameter	Fitted value	U_{fit}	$\%U_{fit}$
$R\delta$	-4.741	0.335	7.07
β / δ	0.126	0.010	7.88

The drift angle and its corresponding uncertainty does not seem affected by the use of weight factors. The modelled turning radius is marginally affected, but its uncertainty is less. This can be explained by the simplification of the weight factors, which decreased the importance of the outer bounds of the distribution (10% instead of 13.53%), see also Figure F4. Nevertheless, it shows that reduction of samples is an acceptable alternative, as long as the probability distribution of the uncertainties is correctly mimicked.

F.4. Alternative methods

F.4.1. Overview

Even the previously shown simplified method is too complex for presently used manoeuvring models. In the report of the 28th Manoeuvring Committee, some alternative methods are proposed, based on more realistic manoeuvring models, to handle the excessive amount of simulations. In this section these methods are shortly described.

F.4.2. Selection of top sensitivity

The previously described simulations can be limited if only the set of coefficients is varied which has the highest sensitivity. To identify this set, first all coefficients should be varied independently, e.g. by adding $\pm 2U_{fit}$ or by performing a common increase with ±10% of the mean value and analysing the outcome on the

simulated manoeuvre. For the example with the linear manoeuvring model this is rather straightforward, as the sensitivity of each coefficient can be determined analytically, for instance:

$$\frac{\partial(R\delta)}{\partial(N_{ur}-mx_G)} = \frac{Y_{uv}}{Y_{uu\delta}N_{uv}-N_{uu\delta}Y_{uv}} \quad \text{(F14)}$$

In the present example changes in $(N_{ur} - mx_G)$ and N_{uv} have the largest influence on $R\delta$, while the drift angle is most affected by changes in Y_{uv} and $(Y_{ur} - m)$.

F.5. Distribution of the results

In the example, presented in this Appendix, the computation of the steady turning diameter and drift angle during turning was considered.

The uncertainty on the outcome is clearly normal distributed, however, this is not the case for all manoeuvring parameters. For example, the overshoot angles during a zigzag test show rather a Weibull distribution, as can be seen in Figure F5.

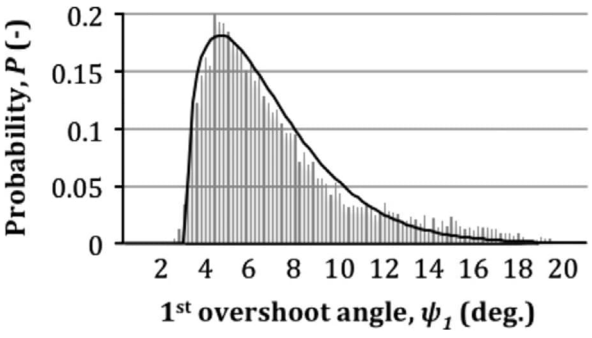

Figure F5: probability distribution of the obtained first overshoot angles after Monte Carlo simulations (Woodward, 2014).

F.6. List of symbols

D	Turning diameter
I_{ZZ}	Yaw moment of inertia
m	Mass
mc	Model coefficients
R	Steady turn radius
s	Number of steps
u, v	Surge and sway velocities
$\dot{u}$, $\dot{v}$	Surge and sway accelerations
x, y, z	Axes
x_G	Longitudinal centre of gravity
X, Y, N	Hydrodynamic forces and moments
β	Drift angle
δ	Rudder angle
μ	Mean of distribution
σ	Standard deviation

Appendix G.
EXAMPLE OF UNCERTAINTY OF CARRIAGE KINEMATICS

G.1. Theory

The example here is elaborated based on the theory explained in Vantorre (1988, 1989, 1992), expressed with the terminology of 7.5-02-01-01.

The trajectory of a ship model is expressed by m mechanism control and setting parameters s_i which give a position $[\boldsymbol{x_0}]$ of the ship in the horizontal plane. For a PMM test these are, in case of a position-controlled carriage:

- The position of the longitudinal carriage s_1;
- The position of the lateral carriage s_2;
- The rotation angle of the yawing table s_3.

and the path is:

$$[\boldsymbol{x_0}] = [s_1 \quad s_2 \quad s_3] \tag{G1}$$

Another example is a circular motion test, where the path is controlled by:

- The radius s_1;
- The angular position s_2;
- The drift angle s_3.

leading to the following dependency:

$$[\boldsymbol{x_0}] = \left[s_1 \cos s_2 \quad s_1 \sin s_2 \quad \frac{\pi}{2} + s_2 + s_3\right] \tag{G2}$$

The actual trajectory will differ from the desired one due to the geometric uncertainties mentioned in 2.3, which cause divergences in the time histories of the setting parameters:

$$s_i(t) = s_i^0(t) + s_i^E(t) \tag{G3}$$

Such divergence can be a harmonic fluctuation:

$$s^E(t) = s_A^E(t)\cos(\alpha\omega t + \varphi) \tag{G4}$$

As a result, the actual path will differ from the intended one, which can be expressed by a Taylor expansion:

$$[\boldsymbol{x_0}] = \left[\boldsymbol{x_0^0}\right] + \left[\boldsymbol{x_0^E}\right] = \left[\boldsymbol{x_0^0}\right] + \sum_{\boldsymbol{n=1}}^{\infty} \frac{\boldsymbol{1}}{\boldsymbol{n!}} \left[\sum_{\boldsymbol{j=1}}^{\boldsymbol{m}} s_j^E \frac{\partial}{\partial s_j}\right]^{\boldsymbol{n}} \left[\boldsymbol{x_0^0}\right] \approx \left[\boldsymbol{x_0^0}\right] + \sum_{\boldsymbol{j=1}}^{\boldsymbol{m}} s_j^E \frac{\partial}{\partial s_j}\left[\boldsymbol{x_0^0}\right] \tag{G5}$$

The uncertainties s_i^E are type B uncertainties and their propagation in the path uncertainty is mostly correlated as can be seen for the circular motion test. In accordance with 7.5-02-01-01, $c_i = \frac{\partial}{\partial s_i}$ are the sensitivity coefficients and the combined standard uncertainty is the linear sum of the uncertainties.

The manoeuvring forces depend on the control parameters (propeller rate, rudder angle, which are further not considered here) and the kinematic parameters:

$$[\boldsymbol{k}] = [u \quad v \quad r \quad \dot{u} \quad \dot{v} \quad]\,\dot{r} \tag{G6}$$

which are different from the desired ones due to the uncertainties s_i^E in the settings:

$$k_i(t) = k_i^0(t) + k_i^E(t) \tag{G7}$$

As a result, the measured manoeuvring forces will also deviate:

$$[\boldsymbol{X}] = [\boldsymbol{X^0}] + [\boldsymbol{X^E}] = [\boldsymbol{X^0}] + \sum_{\boldsymbol{n=1}}^{\infty} \frac{\boldsymbol{1}}{\boldsymbol{n!}} \left[\sum_{\boldsymbol{j=1}}^{\boldsymbol{m}} k_j^E \frac{\partial}{\partial k_j}\right]^{\boldsymbol{n}} [\boldsymbol{X^0}] \approx [\boldsymbol{X^0}] + \sum_{\boldsymbol{j=1}}^{\boldsymbol{m}} k_j^E \frac{\partial}{\partial k_j}[\boldsymbol{X^0}] \tag{G8}$$

G.2. Example for an oblique test

Consider the following mathematical model for the bare hull sway force:

$$Y = (Y_{\dot{v}} - m)\dot{v} + (Y_{\dot{r}} - mx_G)\dot{r} + Y_{uv}uv + (Y_{ur} - m)ur + Y_{v|v|}v|v| + Y_{r|r|}r|r| + Y_{v|r|}v|r| \quad \text{(G9)}$$

Asuming an oblique towing test is performed with a CPMC(Computerised Planar Motion Carriage) with speed controlled towing carriage, in other words the desired setting parameters for such test are:

$$[\boldsymbol{s_0}] = [u_0^0 \quad 0 \quad \beta^0] \quad \text{(G10)}$$

Yielding the following sway force:

$$Y^0 = u_0^{0\,2}\left[Y_{uv}\cos\beta^0 \sin\beta^0 + Y_{v|v|}\sin\beta^0\,|\sin\beta^0|\right] \quad \text{(G11)}$$

A first divergence that can be considered is a constant offset on the carriage speed:

$$k_1^E = \varepsilon \quad \text{(G12)}$$

This constant offset had no effect on the carriage acceleration:

$$k_4^E(t) = 0 \quad \text{(G13)}$$

The uncertainty on the sway force is then:

$$k_1^E \frac{\partial Y^0}{\partial u_0} = \varepsilon\left[2u_0\left(Y_{uv}\,cos\,\beta\,sin\,\beta + Y_{v|v|}\,sin\,\beta\,|sin\,\beta|\right)\right] \quad \text{(G14)}$$

which shows that the relative error on the sway force due to a constant speed offset is twice the relative error of the speed offset.

Consider now a constant offset on the drift angle:

$$k_\beta^E = \beta^E \quad \text{(G15)}$$

The uncertainty on the sway force is then:

$$k_\beta^E \frac{\partial Y^0}{\partial \beta} = \beta^E u_0^{0\,2}\left[Y_{uv}(\cos^2\beta - \sin^2\beta) + Y_{v|v|}(2\cos\beta\,|\sin\beta|)\right] \quad \text{(G16)}$$

Both uncertainties are uncorrelated, so if both occur, the uncertainty on the sway force is the sum of eq. (G14) and eq. (G16).

Now assume that the force on carriage speed is fluctuating harmonically as in eq. (G4). Contrary to eq. (G13) the longitudinal carriage has now a fluctuating longitudinal acceleration

$$k_4^E(t) = -\alpha\omega\boldsymbol{u_A}\,sin(\alpha\omega t + \phi) \quad \text{(G17)}$$

which causes a lateral acceleration on the ship model. The combined uncertainty on the lateral force is:

$$\sum k_j^{(E)} \frac{\partial}{\partial k_j}[Y] = u_A\cos(\alpha\omega t + \phi)\left[2u_0\left(Y_{uv}\cos\beta\sin\beta + Y_{v|v|}\sin\beta\,|\sin\beta|\right)\right] + \underbrace{-\alpha\omega u_A \sin(\alpha\omega t + \phi)\cdot\sin\beta}_{\text{uncertainty introduced on } \dot{v}}\,(Y_{\dot{v}} - m) \quad \text{(G18)}$$

Contrary to the example in Appendix A, even for a steady test, the full equation has to be considered. To consider the effect of the fluctuating uncertainty the relative uncertainty on the lateral force is integrated over an interval T:

$$\frac{Y^E}{Y^0} = 2\frac{u_A}{u_0}\left[\left(\frac{\sin 2\pi\alpha}{2\pi\alpha} - C_1(\cos 2\pi\alpha - 1)\right)\cos\phi + \left(\frac{\cos 2\pi\alpha - 1}{2\pi\alpha} - C_1\sin 2\pi\alpha\right)\sin\phi\right] \quad \text{(G19)}$$

with

$$C_1 = \frac{1}{2l'}\frac{Y'_{\dot{v}} - m'}{Y'_{uv}}\frac{1}{\cos\beta + \frac{Y'_{v|v|}}{Y'_{uv}}|\sin\beta|} \quad \text{(G20)}$$

$l' = u_0 T / L$ is the number of ship lengths covered during the integration interval.

Hydrodynamic coefficients are non-dimensionalised with respect to ship length.

The relative uncertainty depends on the phase shift φ and has the following upper limit:

$$\left[\frac{Y^E}{Y^0}\right]_{\max} = 2\frac{u_A}{u_0}\frac{\sqrt{2(1-\cos 2\pi\alpha)}}{2\pi\alpha}\sqrt{1+(2\pi\alpha C_1)^2} = 2\frac{u_A}{u_0}f_1(2\pi\alpha; C_1) \quad \text{(G21)}$$

The function f_1 is shown in Figure G1. Irrespective C_1, $f_1(0; C_1) = 1$ and $f_1(2\pi n; C_1) = 0$, in other words fluctuations integrated over an integer number of periods do not affect the test results.

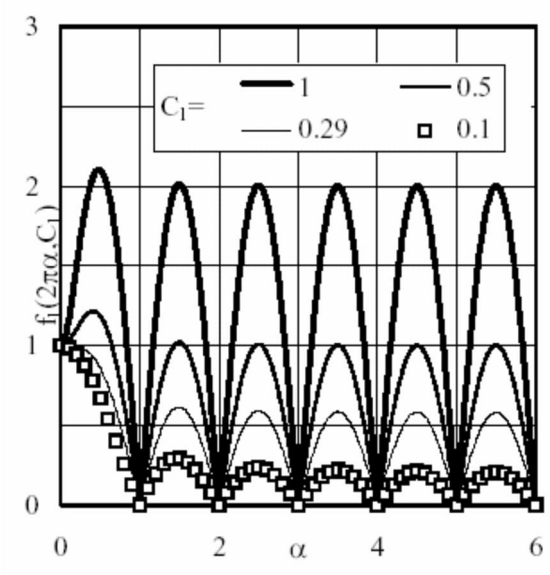

Figure G1: function f_1 for different C_1

The location of the maximum depends on α. For $C_1 = 0.29$ it is reached at $\alpha = 0$ (the static case). For larger C_1 the uncertainty on the force can be larger than the static case.

To analyse the effect with more detail the same dataset as presented in F1 has been used. Table G1 shows the obtained coefficients for the model presented in eq. (G9). Based on Table G1, the following dependencies are found for C_1:

$$\frac{Y'_{\dot{v}} - m'}{Y'_{uv}} = 2.70 \pm 0.19 \quad \text{(G22)}$$

$$\frac{Y'_{v|v|}}{Y'_{uv}} = 7.9 \pm 1.2 \quad \text{(G23)}$$

Table G1. Coefficients for steady state terms.

Derivative	Fitted value	$\%U_{fit}$
$Y_{uu\delta}$	30.164	3.59
Y_{uv}	-428.320	6.57
$Y_{ur} - m$	-240.778	16.81
$Y_{\dot{v}} - m$	-1156.96	2.03
$Y_{\dot{r}} - mx_G$	-202.471	24.45
$Y_{v\|v\|}$	-3374.01	13.06
$Y_{r\|r\|}$	1660.181	89.09
$Y_{v\|r\|}$	-146269	48.45

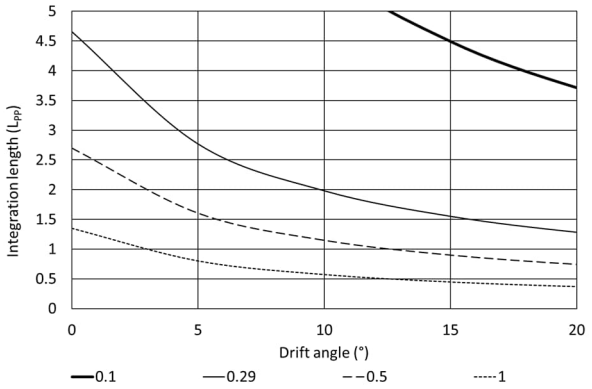

Figure G2: needed integration length to achieve a certain value of C_1, KCS, 20% ukc.

In order to have an uncertainty below the static case, the integration length (for a drift angle of zero degrees), should be at least 5 ship lengths. For the present derivatives, the needed integration length decreases with increasing drift angle.

G.3. Example for a harmonic yaw test

Although a similar methodology can be followed for a complete mathematical model, to reduce the complexity a linear model is used for

this example: the linear yaw model used in Appendix F.

A harmonic pure yaw test can be performed by apposition controlled mechanism which results in the following trajectory:

$$[\boldsymbol{s_0}] = \begin{bmatrix} \frac{u_0^0}{\omega}\int_0^{\omega t}\cos(\psi_A \sin\omega t)d\omega t \\ \frac{u_0^0}{\omega}\int_0^{\omega t}\sin(\psi_A \sin\omega t)d\omega t \\ \psi_A \sin\omega t \end{bmatrix} \quad \text{(G24)}$$

Yielding following reference for the first harmonic of the yawing moment:

$$N^0[1] = N_R^0[1] + iN_I^0[1] = \frac{1}{\pi c}\int_{\varepsilon_R[1]}^{\varepsilon_R[1]+2\pi c} N^0(t)\cos\omega t\, d\omega t + \frac{i}{\pi c}\int_{\varepsilon_I[1]}^{\varepsilon_I[1]+2\pi c} N^0(t)\sin\omega t\, d\omega t = -(N_{ur} - mx_G)u^0\omega\psi_A - i(N_{\dot r} - I_{zz})\omega^2\psi_A \quad \text{(G25)}$$

Yaw table fluctuations are investigated:

$$k_3^E(t) = \psi_A^E\, cos(\alpha\omega t + \phi) \quad \text{(G26)}$$

The propagation of the uncertainty on the cosine and sine components of the yawing moment due to this fluctuation depends on the phase angle ϕ of the fluctuation; again, the upper limit is considered. On the other hand, the integration phase angles $\varepsilon_R[1]$ and $\varepsilon_I[1]$ influence these as well:

$$\left|\frac{N_R^E[1]}{N_R^0[1]}\right|_{max} = \left|\frac{N'_{ur}-N'_{\dot v}}{N'_{ur}-m'x'_G} K f_2(\alpha, c, C_1, C_2)\frac{\psi_A^E}{\psi_A}\right| \quad \text{(G27)}$$

$$\left|\frac{N_I^E[1]}{N_I^0[1]}\right|_{max} = \left|\frac{N'_{ur}-N'_{\dot v}}{N'_{\dot r}-I'_{zz}}\frac{1}{\omega'} K f_2(\alpha, c, C_1, C_2)\frac{\psi_A^E}{\psi_A}\right| \quad \text{(G28)}$$

The value of K is as follows:

- $K = 1$ for $\varepsilon_R[1] = \left(j + \frac{1}{2}\right)\pi$ and $\varepsilon_I[1] = j\pi$;
- $K = \alpha$ for $\varepsilon_R[1] = j\pi$ and $\varepsilon_I[1] = \left(j + \frac{1}{2}\right)\pi$.

The function f_2 is equal to $f_2 =$

$$\left|\frac{2\alpha^2}{\alpha^2-1}\frac{\sqrt{2(1-\cos 2\pi c\alpha)}}{2\pi c\alpha}\sqrt{1 + \left[2\pi\alpha C_1 + \frac{C_2}{2\pi\alpha}\right]^2}\right| \quad \text{(G29)}$$

with parameters C_1 and C_2:

$$C_1 = \frac{N'_{\dot r} - I'_{zz}}{N'_{ur} - N'_{\dot v}}\frac{\omega'}{2\pi}; \quad \text{(G30)}$$

$$C_2 = \frac{N'_{uv}}{N'_{ur} - N'_{\dot v}}\frac{2\pi}{\omega'}. \quad \text{(G31)}$$

In the frame of SIMMAN 2014 harmonic yaw repeat tests were carried out with harmonic yaw period of 38.6 s and 0.62 m/s, thus $\omega' = \frac{\omega L}{V} = 1.15$. The function f_2 is plotted for this dimensionless frequency in Figure G3 using the coefficients of Tables F1 and F2.

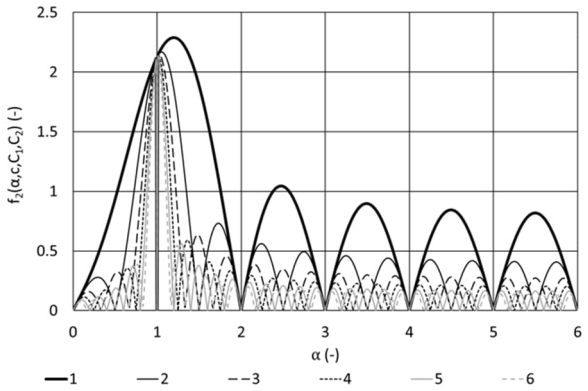

Figure G3: effect of the number of cycles and fluctuation rate on f_2, KCS, 20% UKC.

A distinction can be made based on the frequency of the yaw table fluctuations. For large α, the function f_2 becomes:

$$\lim_{\alpha\to\infty} f_2 = 2\sqrt{2(1-\cos 2\pi c\alpha)}\frac{C_1}{c} \quad \text{(G32)}$$

In other words, f_2 varies between 0 and $\frac{4C_1}{c}$. The influence of high frequent fluctuations decreases with increasing number of cycles c and decreasing test frequency ω'. According to equations (G27) and (G28), the effect can be diminished by choosing appropriate phase angles $\varepsilon_R[1]$ and $\varepsilon_I[1]$ for the integration.

The effect of low frequency fluctuations is maximal for a value α which depends on the number of cycles c and is equal to 1 when $c \to \infty$, in other words fluctuations which vary with the test frequency ω' will have the most severe effect. At that point the function f_2 becomes:

$$\lim_{\alpha \to 1} f_2 = \sqrt{1 + \left[2\pi C_1 + \frac{C_2}{2\pi}\right]^2} \qquad \text{(G33)}$$

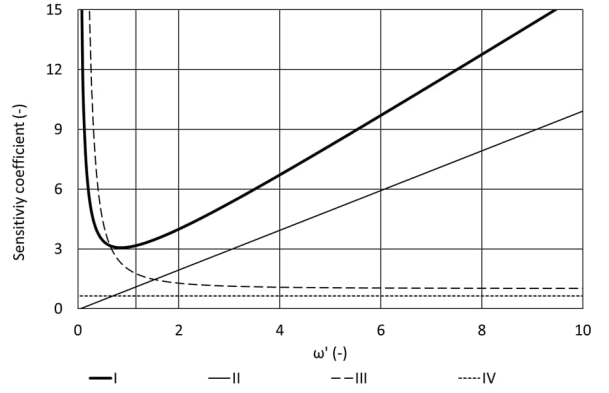

I	$\left\|\frac{N_R^E[1]}{N_R^0[1]}\right\|_{max} \div \frac{\psi_A^E}{\psi_A}, \alpha = 1$
II	$\left\|\frac{N_R^E[1]}{N_R^0[1]}\right\|_{max} \div \frac{\psi_A^E}{\psi_A}, \alpha \to \infty, c = 1, K = 1$
III	$\left\|\frac{N_I^E[1]}{N_I^0[1]}\right\|_{max} \div \frac{\psi_A^E}{\psi_A}, \alpha = 1$
IV	$\left\|\frac{N_I^E[1]}{N_I^0[1]}\right\|_{max} \div \frac{\psi_A^E}{\psi_A}, \alpha \to \infty, c = 1, K = 1$

Figure G4: sensitivity coefficients for the yaw rate fluctuations induced yaw moment (1st harmonic) as a function of test frequency, KCS, 20% UKC.

Figure G4 shows the sensitivity coefficients for the limiting cases as a function of test frequency. $\omega' = 1.15$ is marked by a double vertical line. In general, the imaginary part of the first harmonic of the yaw moment will be less sensitive with increasing test frequency, whereas for the real part the opposite is true. On the other hand, frequency fluctuations with the test frequency will have the largest sensitivity. The SIMMAN 2014 frequency seems to be close to the minimum sensitivity.

G.4. Example for a harmonic sway test

The higher order mathematical model (G9) is now applied for a harmonic sway test, which suffers from lateral position fluctuations:

$$[\boldsymbol{s_0}] = \begin{bmatrix} u_0^0 t \\ y_A \sin \omega t \\ 0 \end{bmatrix} \qquad \text{(G34)}$$

$$k_2^E(t) = y_A^E \cos(\alpha \omega t + \phi) \qquad \text{(G35)}$$

The sensitivity functions are:

$$\left|\frac{Y_R^E[1]}{Y_R^0[1]}\right|_{max} = \left| K \frac{1}{1 + \frac{8}{3\pi}\frac{Y'_{v|v|}}{Y'_{uv}}\omega' \; y_A'} f_1(\alpha, c, C_1) \frac{y_A^E}{y_A} \right| \qquad \text{(G36)}$$

$$\left|\frac{Y_I^E[1]}{Y_I^0[1]}\right|_{max} = \left| K \frac{f_1(\alpha, c, C_1)}{2\pi C_1} \frac{y_A^E}{y_A} \right| \qquad \text{(G37)}$$

As for the yawing moment, the integration phase angles $\varepsilon_R[1]$ and $\varepsilon_I[1]$ influence these as well. The value of K is as follows:

- $K = 1$ for $\varepsilon_R[1] = \left(j + \frac{1}{2}\right)\pi$ and $\varepsilon_I[1] = j\pi$;
- $K = \alpha$ for $\varepsilon_R[1] = j\pi$ and $\varepsilon_I[1] = \left(j + \frac{1}{2}\right)\pi$.

The function f_1 is equal to $f_1 =$

$$\left|\frac{2\alpha^2}{\alpha^2-1}\frac{\sqrt{2(1-\cos 2\pi c\alpha)}}{2\pi c\alpha}\sqrt{[1+C_3 f_*(\alpha)]^2+[2\pi\alpha C_1]^2}\right| \quad \text{(G38)}$$

with parameters

$$C_1 = \frac{\omega'}{2\pi}\frac{Y_{\dot{v}}' - m'}{Y_{uv}'} \quad \text{(G39)}$$

$$C_3 = \frac{4}{\pi}\frac{Y_{v|v|}'}{Y_{uv}'}\omega' \quad y_A' \quad \text{(G40)}$$

The function $f_*(a)$ represents the following series:

- For $K = 1$:

$$f_*(\alpha) = f_{Rc}(\alpha) = -(\alpha^2 - 1)\sum_{k=-\infty}^{\infty}\frac{1}{[(a+2k)^2-1](4k^2-1)} \quad \text{(G41)}$$

$$f_*(\alpha) = f_{Is}(\alpha) = -(\alpha^2 - 1)\sum_{k=-\infty}^{\infty}\frac{(-1)^k}{[(a+2k)^2-1](4k^2-1)} \quad \text{(G42)}$$

- For $K = \alpha$

$$f_{*R}(\alpha) = f_{Rs}(\alpha) = -\frac{(\alpha^2-1)}{\alpha}\sum_{k=-\infty}^{\infty}\frac{(-1)^k(a+2k)}{[(a+2k)^2-1](4k^2-1)} \quad \text{(G43)}$$

$$f_{*I}(\alpha) = f_{Ic}(\alpha) = -\frac{(\alpha^2-1)}{\alpha}\sum_{k=-\infty}^{\infty}\frac{(a+2k)}{[(a+2k)^2-1](4k^2-1)} \quad \text{(G44)}$$

These functions are represented in Figure G5.

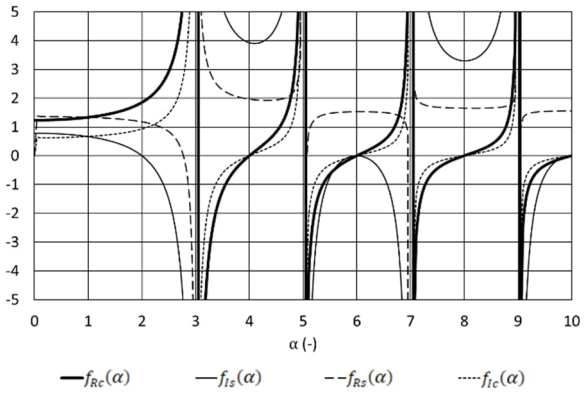

Figure G5: plot of the functions $f_*(\alpha)$

If one considers a small sway velocity, $\omega' y_A' \to 0$ or only a linear model $Y'_{v|v|} = 0$ the complexity of the equations decreases drastically, however, here the effect of these higher order terms is demonstrated.

The SIMMAN 2014 harmonic sway tests have been carried out at 0.62 m/s, with periods of 50.7s and 25.3s and position amplitude of 0.2 m. The derived quantities for each test are shown in Table G2.

Table G2. Parameters for the harmonic sway test.

T (s)	v(m/s)	ω'	C_1	C_3
50.7	0.025	0.87	0.375	0.40
25.3	0.050	1.75	0.752	0.80

The sensitivity coefficients acting on the measured harmonics of the sway force have been plotted in Figure G6 (real part) and Figure G7 (imaginary part). Again, fluctuations around the test frequency have the largest sensitivity.

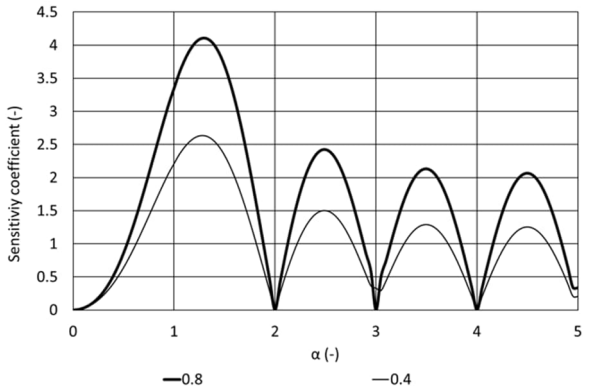

Figure G6: sensitivity coefficients for the sway motion fluctuations induced sway force (Real part of the 1st harmonic) as a function of fluctuation frequency, KCS, 20% UKC, 1 cycle, two different C_3 values.

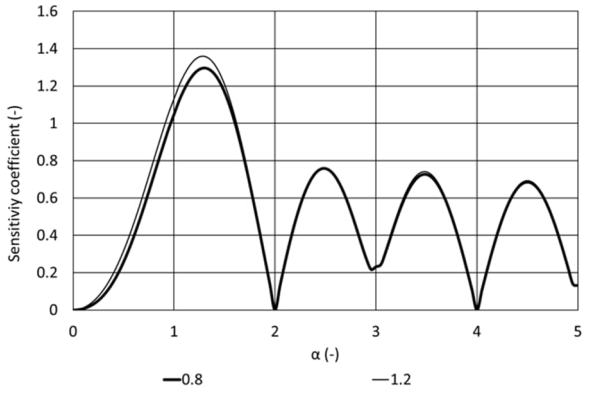

Figure G7: sensitivity coefficients for the sway motion fluctuations induced sway force (Imaginary part of the 1st harmonic) as a function of fluctuation frequency, KCS, 20% UKC, 1 cycle, two different C_3 values.

The effect of C_3 is especially visible on the imaginary part, see Figure G8, where C_3 was increased by increasing the motion amplitude to 5.7 (0.7 m motion amplitude). In this case the sensitivity will have an overall increase, but especially on the third harmonic this increase is visible.

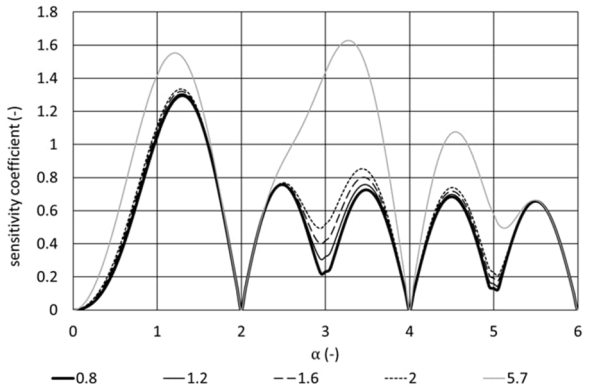

Figure G8: sensitivity coefficients for the sway motion fluctuations induced sway force (Imaginary part of the 1st harmonic) as a function of fluctuation frequency, KCS, 20% UKC, 1 cycle, effect of increasing motion amplitude (increasing C_3 values).

G.5. Conclusions and recommendations

The effect of speed fluctuations has been investigated. This effect depends on the ratio of the different components of the manoeuvring model and the type of manoeuvring model. For oblique tests, the effects can be minimized by increasing the measurement length. This is especially true for the smallest drift angles.

PMM tests are characterised by more parameters and the derivation of the sensitivity coefficients is a complex process, however, one should take care of:

- The test frequency should not be too high.
- Fluctuations with test frequency can be very adverse.
- For a 2nd order model, this is also the case for fluctuations according to the 3rd harmonic of the test frequency.

G.6. List of symbols

c_i	Sensitivity coefficient
I_{ZZ}	Yaw moment of inertia
l'	Non-dimensional number of ship lengths
L	Length
m	Mass

N Hydrodynamic yaw moment
s_i Setting parameters
s_i^E Type B uncertainties
t Time
T Period
u, v, r Surge, sway and yaw velocities
$\dot{u}, \dot{v}, \dot{r}$ Surge, sway and yaw accelerations
x_0 Position in x
x_G Longitudinal centre of gravity
Y Hydrodynamic sway force
α Order of harmonic fluctuation
β Drift angle
$\varepsilon_I, \varepsilon_R$ Integration phase angles
ϕ Phase
ψ Heading
ω Frequency
ω' Dimensionless frequency

G.7. References

Vantorre, M., 1988, "On the influence of the accuracy of planar motion mechanisms on results of captive manoeuvring tests", Scientific and Methodological Seminar on Ship Hydrodynamics, 17th session, Varna, Bulgaria, Vol. 1, p.28.1-8.

Vantorre, M., 1989, "Accuracy considerations and optimization of parameter choice of captive manoeuvring tests with ship models" (in Dutch), DSc thesis, Ghent University, Ghent, Belgium.

Vantorre, M., 1992, "Accuracy and optimization of captive ship model tests", 5th International Symposium on Practical Design of Ships and Mobile Units, Newcastle upon Tyne, UK, Vol. 1, p.1.190-1.203.